Title

The YAP/TAZ antagonist, PTPN14, stabilizes SMAD4 through direct interactions in endothelial cells: Implications for Hereditary Hemorrhagic Telangiectasia

Authors

Ons Mamai, PhD[1], Daniah T. Beleford PhD, MD[1,2], Mark Taylor, PhD[1], Sugandha Basu, MS[1], Xinjian Cen[1], Suprita Trilok, MS[1], Jiamin Zhang PhD[4], Allan Balmain, PhD[1,3], Rosemary J. Akhurst, PhD[1,5*]

[1]Helen Diller Family Comprehensive Cancer Center, University of California, San Francisco, San Francisco, CA, USA

[2]Department of Pediatrics, Division of Medical Genetics, University of California at San Francisco, San Francisco, CA, USA

[3]Department of Biochemistry and Biophysics, University of California at San Francisco, San Francisco, CA, USA

[4] Department of Cancer Genetics and Genomics, Roswell Park Comprehensive Cancer Center, Buffalo, NY, USA

[5]Department of Anatomy, University of California at San Francisco, San Francisco, CA, USA

Short Title: PTPN14 stabilizes SMAD4 in endothelial cells

*Correspondence should be addressed to: R. J. A.

Rosemary J. Akhurst, PhD
Helen Diller Family Comprehensive Cancer Center and Department of Anatomy
1450 3rd Street, San Francisco, CA 94158-9001, USA
Tel 415 514 0215
Fax 415 502 3179
Email: Rosemary.Akhurst@ucsf.edu

ABSTRACT

Hereditary Hemorrhagic Telangiectasia (HHT) is a vascular condition caused by germline heterozygous loss-of-function mutations of *ENG, AVCRL1*, and occasionally *SMAD4*, encoding components of TGFβ/BMP signaling. Telangiectases occur in most HHT patients, and pulmonary, visceral, or cerebral arteriovenous malformations (AVMs) occur in 20-50%, but our understanding of how HHT mutations disrupt down-stream signaling pathways causing clinical manifestations, and why some patients suffer more serious sequelae, is incomplete. We previously showed that genetic variation within *PTPN14* at *rs2936018* associates with presentation of PAVM in HHT patients. Here we show *rs2936018* is a *cis-eQTL* for *PTPN14,* with lower expression of the HHT at-risk allele, and that in primary human endothelial cells, PTPN14 physically interacts with the transcription factor, SMAD4, protecting it from ubiquitylation to support higher SMAD4 expression levels.

In a panel of 69 lung samples, we find *Ptpn14* RNA expression correlates with markers of angiogenesis, lymphangiogenesis, cell-cell interaction, BMP signaling and rho kinase signaling, indicating preferential expression in endothelial cells. RNAScope *in situ* hybridization analysis and use of transgenic *Ptpn14*-reporter mice (*Ptpn14.tm1(KOMP) Vlcg*) show that *Ptpn14* is predominantly but not exclusively expressed in lymphatic and vascular ECs of lung, heart and skin. In lung, *Ptpn14, Acvrl1, Eng* and *SMAD4* expression are tightly correlated as well as with *Flt1, Ece1, Sash1,* and *Mapk3k*. Additionally, *Ptpn14, Acvrl1, Eng* and *SMAD4* show strong expression correlation with components of G protein coupled receptor (GPCR) signaling pathways impacting rho kinase, Cdc42, a regulator of cell migration. We report, for the first time, that in primary

human endothelial cells PTPN14 binds SMAD4, as demonstrated by co-immunoprecipitation studies and confirmed by proximity ligation assay. In the nucleus, PTPN14 stabilizes SMAD4, protecting it from ubiquitylation and turnover and potentiating basal transcriptional activity from BMP and TGFβ responsive reporters, whereas in the cytoplasm PTPN14 sequesters phospho-TAZ (pTAZ) leading to TAZ turnover. PTPN14 therefore provides a physical link supporting BMP/ALK-1/SMAD4 signaling while inhibiting YAP/TAZ signaling in ECs to regulate a balance between these two pathways to maintain vascular stability. Polymorphisms in *PTPN14* may alter tonic BMP/ALK-1/SMAD4 and TGFβ/TGFβRI/SMAD4 signaling to magnify ligand-mediated responses. In this way, genetic variation within *PTPN14* may influence clinical outcomes of HHT through its action on SMAD4.

INTRODUCTION

Hereditary Hemorrhagic Telangiectasia (HHT) patients often present during adolescence with mucocutaneous telangiectases and frequent severe episodes of epistaxis[1, 2]. Telangiectases arise through abnormal vascular remodeling, resulting in capillary breakdown that leads to direct shunting from arterioles into venules without intervening capillary beds[3]. The blood vessel walls of telangiectases are dilated and weak leading to frequent hemorrhage and epistaxis. Bleeding from gastrointestinal tract telangiectases can result in severe anemia that requires repeated blood transfusion. Approximately half of HHT patients also develop larger arteriovenous malformations (AVMs) in lung, brain, and liver that can have more serious clinical sequelae. Like telangiectases, AVMs cause direct shunting of blood from artery to vein that can result in local tissue hypoxia and ischemia and AVMs are prone to hemorrhage. Brain AVMs are often asymptomatic but can cause sudden seizures or hemorrhage. Pulmonary AVMs may cause chronic hypoxemia and exercise intolerance due to impaired gas exchange, and stroke or brain abscess due to pulmonary right to left shunting that can cause paradoxical emboli of both thrombotic and septic origin.

HHT is an autosomal dominant genetic condition with an incidence of 1 case per 5,000 worldwide, and more than 80% of cases are caused by heterozygous loss of function mutations in either *ENG* (HHT type 1) or *ACVRL1* (HHT type 2) that encode endoglin and activin receptor-like kinase-1 (ALK-1), respectively[1, 2]. Loss of function of *SMAD4*, that also causes Juvenile Polyposis Syndrome (JPS/HHT), accounts for some 2% of HHT cases, while additional loci have been implicated in HHT including *GDF2*, that encodes BMP9 and causes HHT type 5[4]. *ENG, ACVRL1* and *SMAD4* have been

added to the American College of Medical Genetics list of reportable secondary sequence findings based on significant clinical evidence that pathogenic variants result in high likelihood of severe disease that may be preventable if identified before symptoms arise[5].

The known causative HHT genes encode components of the TGFβ/BMP signal transduction pathway. Endoglin, encoded by *ENG,* is a trans-membrane glycoprotein related to the TGFβ type III receptor, betaglycan. It has been reported to bind several different TGFβ superfamily ligands, including BMP9 and TGFβ1[6] and it has two alternative spliced protein isoforms that differ in their short cytoplasmic tails[7]. The *ENG* gene is positively regulated by BMP/SMAD signaling[8-10]. Under pathological situations, such as preeclampsia or inflammation, endoglin may be shed from the cell surface by metalloproteases resulting in soluble circulating S-endoglin[11, 12] that can act as a ligand trap. *In vivo* and *in vitro* endoglin regulates endothelial cell (EC) shape, directional migration of ECs against blood flow during development, consequently influencing EC location and maintenance of arterial identity[13, 14]. ALK-1, encoded by *ACVRL1*, is a transmembrane type I receptor kinase that signals for TGFβ and BMP, with preferential binding and activation by BMP9[15]. After ligand binding, ALK-1 phosphorylates and activates SMAD1, 5 and 8, receptor-associated SMADs (R-SMADs) of the BMP pathway. Finally, SMAD4, is a transcription factor that binds phosphorylated R-SMADs of both the BMP (SMAD1, 5 and 8) and TGFβ/activin/nodal (SMAD2 and 3) signaling pathways, and shuttles to the nucleus as part of a SMAD4/SMAD-R hexameric complex to instigate context-dependent transcriptional outputs[16].

Although the genes known to cause HHT have been identified and characterized[1, 2, 4], there is incomplete knowledge of the molecular pathways leading to HHT lesions. Filling this knowledge gap might ultimately result in novel therapeutic strategies for HHT or other vascular disorders. Towards this goal, we previously searched for genetic variants that protect or predispose to more severe phenotypes of HHT[17]. We found genetic association between single nucleotide polymorphisms (SNPs) in the *PTPN14* gene and manifestation of pulmonary AVMs, which occur in 10-50% of patients with HHT1 and HHT2[17]. Based on that finding and on evidence of angiogenesis-suppressing activity of PTPN14 in human primary ECs *in vitro,* we proposed that PTPN14 functionally interacts with the BMP9/ALK-1/endoglin pathway[17], but the molecular mechanism of this interaction has not yet been reported.

PTPN14 (protein-tyrosine phosphatase, non-receptor-type, 14, OMIM 613611) is a member of both the FERM family and the non-receptor tyrosine phosphatase family of proteins. Its carboxy-terminal phosphatase domain has been shown to be involved in dephosphorylating targets of Src kinase, including β-catenin, VE-cadherin, caveolin-1, focal adhesion kinase and other proteins involved in cell-cell and cell-extracellular matrix interactions[18-21]. The molecular mechanisms of its phosphatase activity are not entirely understood since crystal structure and biochemical assays suggest that PTPN14 is an inactive phosphatase[22, 23]. In epithelial cells, independent of its phosphatase activity, PTPN14 is a negative regulator of the Hippo–YAP/TAZ mechano-signal transduction pathway by binding to YAP1 WW motifs through its centrally-located PPxY motifs, causing cytoplasmic sequestration and turnover of YAP1[24-28]. However, in ECs less is known about molecular interactions of PTPN14 with YAP1 or TAZ or with

components of the BMP signaling pathway. Here we show, for the first time, that in primary human endothelial cells, PTPN14 binds to SMAD4. In the nucleus, PTPN14 stabilizes SMAD4, protecting it from ubiquitylation and turnover, whereas in the cytoplasm it sequesters phospho-TAZ (pTAZ) leading to TAZ turnover. We therefore find that PTPN14 provides a physical link supporting BMP/ALK-1/SMAD4 signaling while inhibiting YAP/TAZ signaling in ECs to maintain vascular quiescence.

RESULTS

rs2936018 is a cis-eQTL for PTPN14.

We previously showed that genetic variation within *PTPN14* associates with the presence of pulmonary AVM in HHT patients. Specifically, the common hap-tag SNP, *rs2936018,* showed strongest genetic association with AVM[17]. Here we show using GTEX data[29] that *rs2936018* is a *cis-eQTL* for *PTPN14,* wherein the PAVM-protective minor allele (T) associates with higher *PTPN14* expression levels in human aorta ($P = 3.8 \times 10^{-6}$) (**Supplementary Figure S1**). Moreover, *rs2936018* is localized within a 4Kb intron (intron 11) harboring a cluster of SNPs within and around CTCF binding sites and other regulatory elements, each of which associates with *PTPN14* expression levels in aortic and other tissues. *rs2270703,* 1Kb proximal to *rs2936018,* is a rarer but very strong *cis-eQTL* for *PTPN14* expression levels in human arterial ($P<10^{-10}$ in tibial artery; $P<10^{-6}$ in aorta) and other tissues ($P = 1.6 \times 10^{-100}$ *RE2 Meta-Analysis* of all tissues), wherein the minor allele has lower *PTPN14* expression in all tissues (**Supplementary Figure S1**). This data provides further correlative evidence that genetic variation in

PTPN14 might influence vascular phenotypes, such as clinical features of HHT, through differential expression of the encoded transcripts.

Ptpn14 expression in lung correlates with markers of angiogenesis, vascular remodeling and endocytic recycling.

To shed further light on the functional role(s) of *Ptpn14* in lung, we made use of an F1 inter-species mouse backcross between *Mus spretus* and *Mus musculus* FVB/N (**Figure 1A**). This genetic cross provides greater inter-individual genetic heterogeneity than that observed within the human population, such that each gene shows a wider dynamic range of expression permitting more powerful gene expression correlation analysis[30-33]. We undertook such an analysis using bulk lung RNAs from 69 individual wildtype but genetically heterogenous mice generated from this F1 backcross. Within the top 150 genes showing strong correlation with *Ptpn14* expression (at *rho* ≥ *0.54; z score >3.5; P< 0.0003*), gene ontology (GO) enrichment analysis revealed enhanced contributions from genes involved in angiogenesis, cardiovascular morphogenesis, protein phosphorylation pathways, BMP signaling, rho kinase signaling, cell-cell interactions and endocytosis (**Supplementary Table S1**). 63% of the *Ptpn14*-correlated gene-set (95 of 150 genes) exhibited strong expression correlation with *Eng* or *Acvrl1* (**Figure 1B**), with a core of 47 *Ptpn14*-associated genes highly correlated with *both Eng* and *Acvrl,* the endothelially-expressed HHT causative genes (**Figure 1C; Supplementary Table S2**).

We then scored the magnitude of expression correlation between each of the 150 *Ptpn14*-associated genes with each other and undertook unsupervised hierarchical

cluster analysis based on the *rho* value for each pair-wise gene comparison (**Figure 1D).** This revealed four gene clusters (**Figure 1D; Supplementary Table S3**) and GO enrichment analysis was undertaken for each cluster (**Figure 1E**). Cluster A shows strong enrichment for genes of angiogenesis, endothelial cell differentiation, focal adhesion, lymphangiogenesis and venous differentiation (including *Ptpn14*, *Acvrl1*, *Notch1*, and *Amotl2*), and Cluster D shows significant enrichment for genes involved in angiogenesis, cardiovascular morphogenesis, VEGF responses and PI3K signaling (including *Eng, Dll4, Map3k3, Flt1, and Flt4)*. Cluster B is enriched for Rho protein signaling, TGFβ receptor complex assembly, integrin mediated signaling and epicardial-to-mesenchymal cell transition. Finally, Cluster C is enriched for processes of protein trafficking within the ER and Golgi apparatus, assembly of clathrin-coated pits and endocytosis (**Fig. 1E**).

Smad4, the third HHT-causative gene*,* that is more widely expressed than *Eng or Acvrl1,* also showed expression correlation with *Ptpn14* (*rho = 0.50*)*,* albeit just below the threshold we set for selection of the 150 gene-set (*rho ≥ 0.54).* Notably, of the 47 lung transcripts tightly correlated with *Eng, Acvrl1,* and *Ptpn14 (at rho > 0.54),* thirteen were also strongly associated with *Smad4* expression (*at rho ≥ 0.54:* **Figure 1C**, and **Supplementary Table S4**). The strongest of these associations was with *Flt1,* encoding FLT/VEGFR1; *Ece1,* encoding endothelin-converting enzyme 1*; Mek3k3* and *Sash1,* that are, respectively, reportedly involved in hippo signaling, stress-activated protein kinase signaling, and regulation of NFkB activation[34, 35].

Eight of the thirteen genes with strong association to each of our four seed genes, *Eng, Acvrl1, Smad4*, and *Ptpn14,* encode components of G protein coupled

receptor (GPCR) signaling pathways, particularly related to Cdc42 rho kinase signaling that influences cytoskeletal regulation, cell adhesion and migration**.** These include i) three G protein coupled receptors, E2 (CD97), L3 (Latrophilin 3), and F5, encoded by *Adgre2, Adgrl3,* and *Adgrf5,* respectively; ii) the guanine nucleotide exchange factor, *Dock9,* that activates Cdc42; iii) three GTPase activating proteins that are negative regulators of the GTPases Cdc42 and Rac1, namely Cdc42 GTPase-activating protein (*Cdgap* or *Arhgap31*), *Stard8 (Dlc2)*[36] and *Stard13 (Dlc3)*[37]; and iv) *Cds2* (CDP-diacylglycerol synthase 2)*,* which regulates the amount of phosphatidylinositol downstream of GPCR signaling by catalyzing the conversion of phosphatidic acid to CDP-diacylglycerol. The 13th gene, *Prdm16*, encodes a transcriptional regulator involved in brown fat metabolism, that has recently been shown to protect from cardiovascular aging[38].

Notably, despite use of bulk lung RNA analysis, most of the *Ptpn14*-correlated genes and clusters are associated with vascular rather than epithelial structures and processes. The only epithelial marker associated with *Ptpn14* at the stringency used is *Krt19,* a simple type I keratin that is expressed in stem cells (**Supplementary Table S3**). Overall, gene expression network analysis provides strong correlative support for a role for *PTPN14* in interacting with HHT pathway components in vascular cell adhesion and migration in the lung.

PTPN14 is expressed in lung and heart ECs *in vivo*

Most functional studies on PTPN14 have focused on its role in epithelial cells, where it is a negative regulator of YAP by binding, sequestering and turning over phosphorylated YAP1 in the cytoplasm[24-27]. *PTPN14* is also a p53 target gene and acts as a tumor suppressor during carcinoma development[20, 39, 40]. Since our lung expression data suggest involvement in endothelial cells, we examined *Ptpn14* RNA expression in lung and other tissues by two color chromogenic *in situ* hybridization analysis using RNAScope® with differentially labeled probes for *Ptpn14* (blue) and *Eng* (pink), the latter being an EC marker. In early embryos, *Ptpn14* was observed in *Eng*-positive blood vessels and blood islands within the 8.5 days *post-coitum* yolk sac and in *Eng*-negative neuroepithelium (**Figure 2A,B**). In adult lung, *Ptpn14* RNA was co-expressed with *Eng* in ECs of small vessels and alveoli but was also detected at high levels in *Eng*-negative bronchial epithelial cells (**Figure 2C, D).** Preferential expression of *Ptpn14* in ECs of adult lung is supported by analysis of single cell RNA-seq data[41-43] wherein ECs express highest *Ptpn14* levels, with sequentially lower expression in mesenchymal, epithelial, and immune cells of both mouse and human lung (**Supplementary Figure S2.**). In the cardiovascular system, *Ptpn14* and *Eng* transcripts were co-expressed in endocardial cells, particularly of the left atrium, and in ECs of the aorta and coronary capillaries, for example within the myocardium of the left ventricle (**Figure 2E,F**). *RNAScope* analysis using non-specific probes showed no signal (**Supplementary Figure S3**).

To complement the above findings, we utilized *Ptpn14.tm1(KOMP)Vlcg* mice[44], henceforth termed *Ptpn14-LacZ*, a transgenic line that drives β-galactosidase

expression from the endogenous *Ptpn14* gene promoter (MGI:5695871). β galactosidase activity was observed as a blue stain within ECs of the lung, with prominent staining of lymphatic ECs (**Figure 3A,B**), and lesser staining in blood vessel ECs (**Figure 3C**). In skin, we observed strong staining in lymphatic ECs (not shown) and ECs of subcutaneous blood vessels in muscle tissue (**Figure 3D,E**) and adipose (**Figure 3F**). ECs on the semi-lunar heart valves, particularly on the aortic face of the valve leaflet showed strong LacZ staining (**Figure 3G**), as did ECs of coronary vessels (**Figure 3H**). Curiously, there was no staining of bronchial epithelial cells, despite the *Ptpn14* signal observed using RNAScope® analysis (Figure **2C,D**).

PTPN14 enhances endoglin, ALK-1 and SMAD levels in primary human ECs

To investigate possible interactions between PTPN14 and the BMP9/ALK-1 signaling pathway in ECs, we examined the effects of *siRNA*-mediated knockdown (KD) of *ENG (siENG)*, *ACVRL1 (siALK1)*, and *PTPN14* (*siP*) on one another's protein level and on downstream signaling components of the BMP9 signaling pathway in low passage primary human umbilical arterial ECs (HUAECs). Because *PTPN14* expression is highest at high cell density[24], HUAECs were transfected with *siRNAs* and cultured to >90% density before treatment with BMP9 to mimic conditions of a stable vascular endothelial monolayer.

In control HUAECs transfected with non-targeting *siRNA* (*siNT*), phosphorylation of SMAD1/5/8 was transiently induced one hour following BMP9 treatment, and this induction was eliminated by prior KD of ALK-1 (*siALK1)*, a SMAD1/5 phosphorylating receptor kinase (**Figure 4A,B**). Endoglin levels were increased 24 hours after exposure

to BMP9, and this was prevented by *siALK1* (**Figure 4A,B**) or *siSMAD4* pre-treatment (**Supplementary Figure S4A**), consistent with the encoding *ENG* gene being a known BMP transcriptional target gene[8-10]. Contrasting with *siALK1*, *siENG* did not fully suppress BMP9-induced SMAD1/5 phosphorylation (**Figure 4A,B**), suggesting that endoglin is not essential for BMP9-induced activation of canonical SMAD1/5 signaling or is only required at very low levels, consistent with observations of others[45, 46] and suggesting that in arterial ECs, endoglin is a predominantly a target of BMP9/ALK-1 signaling rather than a major upstream mediator of signaling (**Figure 4C**). Like the effect of *siENG*, *siPTPN14* decreased BMP9-triggered activation of pSMAD1/5 by around 50% and lowered both the basal and BMP9-induced endoglin and ALK-1 levels (**Figure 4A,B**). *siPTPN14* additionally suppressed protein levels of endoglin and SMAD4 (**Figure 4A,D; Supplementary Figure S4A**).

TGFβ1 also induced phosphorylation of SMAD1 as well as enhancing SMAD4 levels in HUAECs, albeit TGFβ activation of pSMAD1 was less effective than BMP9 (**Figure 4F**). Since this induction was resistant to treatment with the TGFβRI (ALK5) inhibitor, SB-431542, we assume that it is mediated through TGFβR2-ALK-1 signaling[47] (**Figure 4F**). Indeed, SB-431542 potentiated pSMAD1 and SMAD4 levels in the presence of TGFβ, indicating that when TGFβR1 kinase is inhibited, TGFβR2 signaling is diverted down the ALK-1-SMAD1/5 pathway. KD of *PTPN14* reduced induction of SMAD1 phosphorylation by both BMP9 and TGFβ1, suggesting a role for PTPN14 in stabilizing ALK-1 kinase-induced pSMAD1, regardless of the activating ligand or type II receptor (**Figure 4D**).

Endogenous PTPN14 binds and stabilizes SMAD4 in primary HUAECs

Since PTPN14 regulates levels of endoglin, SMAD4 and ALK-1, we tested the possibility that PTPN14 might directly bind and thus stabilize one of these proteins. Neither of the transmembrane proteins, ALK-1 or endoglin, co-immunoprecipitated with endogenous PTPN14 and nor did the inhibitory SMAD7 (**Figure 4G)**. As a positive control, we examined interaction between PTPN14 and YAP1, a well characterized binding partner for PTPN14 in epithelial cells[24-27]. At high cell density, we found that HUAECs do not express YAP1 but TAZ, a YAP1 paralogue, and phosphorylated TAZ co-immunoprecipitated with PTPN14 Interestingly, endogenous pSMAD1/5 and SMAD4 both bound endogenous PTPN14 to a similar extent as binding of PTPN14 to pTAZ (**Supplementary Figure S4B**). In reciprocal co-immunoprecipitations, SMAD4 bound pSMAD1/5, SMAD7, TAZ and PTPN14, as expected (**Supplementary Figure S4C**).

As PTPN14 is involved in endosome recycling and endocytosis[48], we postulated that it may influence SMAD4 levels through ubiquitylation and degradation. *siPTPN14* KD in HUAECs resulted in reduced levels of total SMAD4 but the protein that remained was heavily ubiquitylated. Conversely, *PTPN14*-overexpression enhanced total SMAD4 levels but reduced the amount of ubiquitylated SMAD4 (**Supplementary Figure S4D**). Therefore, PTPN14 appears to promote deubiquitylation of SMAD4 to mediate stabilization of SMAD4.

Stabilization of SMAD4 by PTPN14 occurs within nuclear extracts.

Nucleocytoplasmic fractionation of primary HUAECs revealed that in nuclear lysates SMAD4 was consistently reduced by *siPTPN14*, whereas the effect of *siPTPN14* on cytoplasmic SMAD4 was less consistent, in part due to lower cytoplasmic SMAD4 levels in high density HUAECs (**Figure 5A,B**). In contrast, TAZ was cytoplasmically located in confluent HUAEC cells, with a barely detectable shift from cytoplasm to nucleus following *PTPN14* KD (**Figure 5A**). Despite reduced SMAD4 expression following *PTPN14 KD,* nuclear accumulation of SMAD4 in response to BMP9 still occurred (**Figure 5B)**, suggesting that PTPN14 is not required for this activity, which is consistent with our finding of only 50% reduction in BMP9-induced pSMAD1/5 after *PTPN14* KD (**Figure 4A**).

To further investigate the relationship between PTPN14 and SMAD4, we overexpressed these proteins in HEK293 cells. Notably, co-transfection of SMAD4-FLAG together with increasing quantities of V5-PTPN14 demonstrated that V5-PTPN14 stabilizes the SMAD4-FLAG protein in a dose-dependent manner (**Figure 5C,** left panel). Reciprocal co-immunoprecipitation between SMAD4-FLAG and V5-PTPN14 (**Figure 5C,** three right panels), confirmed our findings of physical interactions between the endogenous proteins observed in primary HUAECs (**Figure 4**). Subcellular fractionation showed that SMAD4-FLAG localizes to both nucleus and cytoplasm, with higher levels in the nucleus (**Figure 5D**), and co-transfection with V5-PTPN14 raised SMAD4-FLAG levels in both nucleus and cytoplasm (**Figure 5D**). Co-immunoprecipitation experiments showed interaction between V5-PTPN14 and SMAD4-FLAG in the nucleus, and this interaction was undetectable in the cytoplasm (**Figure**

5E). Due to the limits of detection of PTPN14 by Western analysis, however, we cannot rule out a physical interaction between SMAD4 and PTPN14 in the cytoplasm.

Endogenous SMAD4-PTPN14 interactions detected by proximity ligation assay in primary HUAECs.

To confirm the presence of molecular interactions between endogenous PTPN14 and SMAD4 proteins in primary HUAECs, we undertook proximity ligation assays (PLAs) using primary antibodies optimized for specificity to each target protein as assessed by immunocytochemistry following siRNA KD (not shown). Using a PCR-based signal initiated by primers that tag distinct secondary antibodies, PLA detects two proteins that are within 40nM proximity to each other within the cell, i.e. presumed to bind one another. As a positive control, we undertook PLA between SMAD4 and pSMAD1/5 that shows PLA signals predominantly in the nucleus, with increased nuclear signal after BMP9 treatment for 1 hour (**Figure 6A,B**). PLA for PTPN14 and SMAD4 interaction showed nuclear and cytoplasmic signal, with more nuclear staining after BMP9 treatment (**Figure 6C,D**). Negative controls included PLA undertaken with only one tagged antibody or using secondary antibodies only to show levels of non-specific background (**Figure 6E-H**). In conclusion, we demonstrate physical interaction between PTPN14 and SMAD4, preferentially within the nucleus of primary HUAECs, by both co-immunoprecipitation and PLA.

PTPN14 enhances SMAD4 levels and potentiates* both *BMP9-inducible and TGFβ inducible gene expression.

The PTPN14 protein has three structural domains, a ~ 300 aa amino terminal FERM domain characteristic of proteins associated with the cytoskeletal cortex (aa 21 to 306), a carboxy-terminal tyrosine phosphatase domain (aa 909 to 1180), and a long proline-rich linker region that spans between these and encompasses at least two PPxY motifs (**Figure 7A**). PPPY at aa 566-569 and PPEY at aa 748-752 are implicated in binding phosphorylated YAP1 to tether it within the cytoplasm for ubiquitylation and subsequent degradation via the proteasome[24-27]. We transfected the various PTPN14 constructs into HEK293 cells to probe domain-specific contributions to SMAD4-PTPN14 interactions. These include wildtype PTPN14 or constructs lacking either the FERM or phosphatase domains, or with mutations in both PPxY domains that prevent binding of pTAZ to PTPN14[25] (**Figure 7A**). Co-transfection of a single dose of FLAG-tagged SMAD4 with increasing quantities of wild type V5-PTPN14 as reported in **Figure 5**, confirmed stabilization of SMAD4-FLAG protein levels (**Figure 7B, C**). The V5-PTPN14-△FERM mutant that lacks the PTPN14 ubiquitylation site(s)[24], showed reduced PTPN14 ubiquitylation and turnover, resulting in high levels of truncated V5-PTPN14-△FERM protein, and far higher SMAD4-FLAG levels (**Figure 7B)**. The V5-PTPN14-ΔPase mutant also enhanced levels of co-transfected SMAD4-FLAG over that of wild type V5-PTPN14 (**Figure 7B**), indicating that neither the FERM nor phosphatase domains of PTPN14 are required for SMAD4 stabilization, but may indeed impede it. Transfection of mPPxY.PTPN14 harboring mutations in its two YAP-binding PPxY motifs, resulted in the highest expression levels of co-transduced SMAD4-FLAG despite

no change in the intrinsic level of input V5-PTPN14 protein following transfection of wildtype *versus* mPPxY.PTPN14 (**Figure 7C, D**).

To determine whether the PTPN14-mediated increase in SMAD4 levels translates into potentiated SMAD4/pSMAD1/5 mediated transcriptional responses, we examined the effects of PTPN14 overexpression or KD (*siP*) on basal expression and BMP9 inducibility of a BMP-response element (BRE)-luciferase reporter in HEK293 cells. Co-transfection of wildtype PTPN14 with the BRE-reporter elevated basal BRE-luciferase activity 1.4 fold compared to no PTPN14 transfection. With no exogenous PTPN14 transfection, BMP9 treatment for 24 hours induced BRE-luciferase reporter activity six-fold (**Figure 7E**). Each PTPN14 mutant construct that potentiated SMAD4 protein levels (**Figure 7B-D**) also elevated basal expression of the BRE-reporter without enhancing the magnitude of induction by BMP9 (**Figure 7E**). The elevated basal BRE-luciferase activity by each PTPN14 construct was resistant to the ALK-1 inhibitor, K02288 (**Figure 7E**), consistent with the concept that PTPN14-driven enhancement of SMAD levels occurs downstream of ALK-1, bypassing a requirement BMP9-induced ALK-1 kinase activity.

Since SMAD4 is a common co-SMAD used by all members of the TGFβ superfamily, we asked whether TGFβ-SMAD2/3 signaling was also affected by PTPN14 expression. Indeed, *PTPN14* KD (siP) significantly reduced basal and TGFβ inducible expression of a PAI-1-luciferase reporter in TMLE cells (**Figure 7F**), whereas transfection of these cells with WT-PTPN14 significantly enhanced both basal and TGFβ-inducible PAI-I-reporter activity, with induced basal expression being resistant to the TGFβR1 inhibitor, SB431542. Elevated SMAD4 levels observed following PTPN14

over-expression therefore translate into enhanced basal BRE-luciferase and PAI-1 luciferase activity, but no change in the magnitude of ligand inducibility. Nevertheless, relatively small modulations in basal SMAD4 protein levels by PTPN14 are transcriptionally and/or translationally amplified such that they significantly alter signaling outputs. Following on from this observation, such changes might suppress or accentuate clinical phenotypes in a pathological setting.

PTPN14, SMAD4 and TAZ interactions in HEK293 cells

Endogenous and ectopic PTPN14 protein is rapidly turned over in HEK293 cells as revealed by use of proteosome inhibitors (**Supplementary Figure S5A),** consistent with its role in endocytic recycling versus proteosomic degradation[48]. To further explore the interactions between *PTPN14, SMAD4,* and TAZ, we undertook co-transfection experiments of V5-PTPN14 with TAZ-HA, as well as co-transfections of these two proteins with FLAG-SMAD4 in HEK293 cells. Wild type V5-PTPN14 destabilized co-transfected TAZ-HA (**Figure 7G lanes 2-5),** as has been reported for the activity of PTPN14 on YAP1[24-26]. Conversely, *siPTPN14* potentiated expression of TAZ-HA (**Supplementary Figure S5B lane3)**, consistent with a role of PTPN14 in TAZ turnover. Compared to WT-PTPN14, V5-PTPN14.mPPxY had reduced activity in stimulating TAZ-HA turnover, concordant with its inability to bind TAZ (**Figure 7G, lanes 6-7**). TAZ-HA somewhat down-regulated endogenous PTPN14 in both the nucleus and cytoplasm (**Figure 7H, Supplementary Figure S5B,C)**, possibly because a fraction of PTPN14 is delivered to the proteosome in complex with pTAZ.

TAZ-HA destabilized SMAD4-FLAG (**Figure 7H, compare lanes 2 and 3)**, and addition of wildtype V5-PTPN14 to this combination destabilized TAZ-HA but did not restore SMAD4-FLAG levels to their previous state (**Figure 7H, lanes 4-6**). However, V5-PTPN14-mPPxY prevented turnover of both TAZ and SMAD4 (**Figure 7H, lane 7**). This could be explained if TAZ normally competes with SMAD4 for binding to PTPN14. For example, if SMAD4 binds PTPN14 within the proline-rich linker region adjacent to, but independent of, the PPxY motifs. TAZ bound to PTPN14 via the PPxY motifs might then exert stearic hindrance on SMAD4/PTPN14 interaction. With WT-PTPN14, TAZ would outcompete SMAD4 for binding PTPN14, leaving SMAD4 unbound and unprotected. With mPPxY.PTPN14 that cannot bind TAZ, PTPN14 is then free to bind and stabilize SMAD4, while TAZ is not degraded since it does not efficiently bind to PTPN14.

Discussion:

PTPN14 is a negative regulator of YAP/TAZ signaling in epithelial cells, and YAP/TAZ has been implicated in HHT[49], but how BMP9-ALK-1-SMAD4 are molecularly connected with YAP/TAZ in HHT has not been determined. We show here, as reported for studies of on YAP/TAZ in epithelia[24-26], that PTPN14 downregulates TAZ in the cytoplasm of quiescent ECs. Most importantly, we show by co-immunoprecipitation and PLA of endogenous proteins that PTPN14 directly binds SMAD4 and enhances SMAD4 levels in quiescent primary HUAECs. Physical association between SMAD4 and PTPN14 occurs predominantly but not exclusively in the nucleus of quiescent cells to potentiate BMP9-induced phosphorylation of Smad1/5. PTPN14 also enhances tonic transcriptional output from a BRE-luciferase reporter to amplify BMP9-induced

transcriptional output. PTPN14 therefore provides a physical link between SMAD4 and YAP/TAZ, orchestrating vascular stability through multiple mechanisms, including sequestration and turnover of pYAP/TAZ in the cytoplasm and support of SMAD4-mediated transcription in the nucleus. Recent studies reveal that PTPN14 can additionally contribute to maintenance of endothelial integrity by dephosphorylation of VE-Cadherin[18]. Together, these findings suggest that PTPN14 acts on multiple molecular pathways to orchestrate stabilization of the quiescent vascular endothelium.

We also show that the haplotype marker, *rs2936018,* associated with AVMs in Dutch and French HHT[17], is a *cis-eQTL* for *PTPN14* expression. The major allele, *rs2936018-C*, associated with AVM-predisposition also associates with lower *PTPN14* expression in arterial tissues. Notably, *rs2936018* is located within a small 4Kb intron of *PTPN14* possessing CTCF binding sites and other regulatory elements, and several SNPs in this intron are *cis-eQTL*s for *PTPN14*. *rs2270703*, a rare SNP located 1Kb proximal to rs2936018 is a strong PTPN14 *cis-eQTL* in multiple human tissues ($p = 5.8 \times 10^{-100}$: RE2 Meta-Analysis), with greatest expression correlation in human arterial tissues.

A recent report found no genetic association of *rs2936018* with the presence of pulmonary AVM in HHT[50]. The population structure of that study was different from ours, namely isolated probands rather than family pedigrees, and by necessity used different statistical approaches. Nevertheless, despite these differences, there was a trend towards genetic association between *rs2936018* and AVM even in that study. This highlights the difficulty of undertaking genetic association studies for modifiers of rare diseases, considering the limitation of small population sizes and genetic heterogeneity.

It is notable that human lung RNA samples within GTEx showed no association between the *rs2936018* or *rs2270703* and *PTPN14* gene expression. This may be due to the limitations of using human lung samples that are derived predominantly from older patients, with variable environmental and pathological status, that result in more variable gene expression data. However, this does highlight the alternative power of using inter-species mouse genetics to screen for variations in gene expression, as this approach permits strict controls over environmental factors, age and gender, as well as a larger dynamic range of gene expression to generate cleaner gene expression data. (This lung expression dataset is available at (to be added on acceptance for publication).

Our lung gene expression network analysis demonstrates the power of inter-specific mouse backcross analysis to identify novel *in vivo* functions of candidate genes. We show *PTPN14*, although showing only marginal human genetic association, nevertheless shows powerful gene expression network interdependence with the major HHT causative genes, *Eng, Acvrl1,* and *Smad4,* in the target organ in question, namely lung. We provide supportive evidence that *PTPN14* is indeed predominantly expressed in ECs of the lung, using RNA *in situ* hybridization analysis with *Eng* and *Ptpn14* and using transgenic reporter mice expressing β galactosidase from the *Ptpn14* gene promoter. Finally, we present strong molecular evidence that these four genes regulate each other's expression in primary human arterial endothelial cells and demonstrate a direct physical interaction between PTPN14 and SMAD4 that stabilizes the latter and potentiates BMP9, ALK-1, SMAD4, endoglin signaling.

The *Tgfbm2/Ptpn14* locus was originally identified as a suppressor of *Tgfb1-/-* embryo lethality. PTPN14 acts on SMAD4, a co-SMAD shared by most TGFβ signaling molecules, and we show here that it modulates both TGFβ and BMP signaling outputs. Our findings here may have broader implications for other superfamily ligands, cell types and diseases, including cancer[39].

Intriguingly our gene expression network analysis shows that eight of the 13 genes with highest gene expression correlations with *Ptpn14, Eng, Acvrl1* and *Smad4*, encode components of GPCR signaling pathways that implicate Cdc42, a small GTPase of the Rho family. Cdc42 is central to dynamic actin cytoskeletal assembly and rearrangement that forms the basis of cell-cell adhesion and migration. It regulates signaling pathways controlling endocytosis, cell shape, morphology, and migration, and can be activated by integrin signaling. Intriguing, Cdc42 has been implicated in mediating the promigratory effect of cytoplasmically-localized YAP/TAZ on endothelial tip cell migration in developing retina[51]. This finding is relevant to our studies on HHT molecular pathogenesis, given our understanding that PTPN14 sequesters YAP/TAZ in the cytoplasm, and that genetic loss of either endoglin, ALK-1, or SMAD4 results in changes in cell shape, including altered size and cellular footprint, and loss of the characteristic directional migration of ECs against blood flow[13, 14, 52-54].

We also found that *Map3k3* expression (encoding Mitogen-Activated Protein Kinase Kinase Kinase 3; MEKK3) is also highly correlated with expression of the four seed genes. MEKK3 and has recently been suggested to activate Hippo signaling at two junctures; by direct phosphorylation and activation of LATS1/2 and YAP-1, and by promoting β-TRCP interaction with YAP to drive YAP ubiquitylation and degradation[34,

[35]. Significantly, MEKK3 is also a mediator of a related but distinct autosomal dominant vascular disorder, Cerebral Cavernous Malformations[55], wherein haploinsufficiency for one of three CCM genes predisposes to development of vascular cerebral cavernous malformations. Normally, a complex of CCM2 and CCM3 binds and inactivates MAPK3K, but in CCM mouse models, vascular malformations can be prevented by genetic loss of *Mapk3k.* Notably, MEKK3 activates both Rho activity[55] and Hippo signaling[35], which would result in cytoplasmic retention of YAP/TAZ. It is therefore intriguing that cytoplasmic but not nuclear YAP/TAZ promotes endothelial tip cell migration through Cdc42[51]. It appears the ALK-1-SMAD4-endoglin and CCM axes may converge on similar pathways that regulate Hippo-YAP/TAZ and Cdc42 rho kinase activity.

Human genetic association data alone is only a first step in interrogating how a candidate gene regulates a human disease process. Yet an understanding of how variant genes regulate the pathobiology of a specific disease, and how they interact with other gene expression networks to regulate *in vivo* biology may provide novel clues for therapeutic approaches. The phosphoprotein substrates of PTPN14 phosphatase activity tend to be substrates of Src kinases, hinting at the use of Src kinase inhibitors as possible drugs to be tested in models of HHT.

Thalidomide and pomalidomide, drugs that target components of the ubiquitylation machinery, are already of use or in clinical trial for HHT therapy[56], and this class of IMiD drugs may affect both PTPN14/SMAD and PTPN14/YAP/TAZ ubiquitylation and turnover. Future design of more specific drugs with fewer side effects, would benefit from knowledge of the interactions that regulate stability of PTPN14,

SMAD4 and YAP/TAZ. A deeper understanding of the interactions between the Hippo-YAP/TAZ pathway, BMP9-ALK-1-SMAD signaling, MEKK3, and Rho GTPase Cdc42 signaling may also provide new drug targets for HHT[57].

Acknowledgments, Sources of Funding, & Disclosures:

We thank Rik Derynck for critical pre-review of the manuscript, and Adila Izgutdina for technical assistance. This work was funded by NIH grants R01-HL122869 and R01CA210561. OM was funded in part by a fellowship from the ADDAX foundation. DTB was funded in part by a UC Presidential Post-doctoral Fellowship. This publication is dedicated to the memory of Mrs Rym Fekih-Romdhane.

The authors have no financial disclosures relevant to this study.

References:

1. Shovlin CL. Hereditary haemorrhagic telangiectasia: pathophysiology, diagnosis and treatment. *Blood Rev*. 2010;24:203-19.

2. Faughnan ME, Palda VA, Garcia-Tsao G, Geisthoff UW, McDonald J, Proctor DD, Spears J, Brown DH, Buscarini E, Chesnutt MS, Cottin V, Ganguly A, Gossage JR, Guttmacher AE, Hyland RH, Kennedy SJ, Korzenik J, Mager JJ, Ozanne AP, Piccirillo JF, Picus D, Plauchu H, Porteous ME, Pyeritz RE, Ross DA, Sabba C, Swanson K, Terry P, Wallace MC, Westermann CJ, White RI, Young LH and Zarrabeitia R. International guidelines for the diagnosis and management of hereditary haemorrhagic telangiectasia. *J Med Genet*. 2011;48:73-87.

3. Guttmacher AE, Marchuk DA and White RI, Jr. Hereditary hemorrhagic telangiectasia. *N Engl J Med*. 1995;333:918-24.

4. Wooderchak-Donahue WL, McDonald J, O'Fallon B, Upton PD, Li W, Roman BL, Young S, Plant P, Fulop GT, Langa C, Morrell NW, Botella LM, Bernabeu C, Stevenson DA, Runo JR and Bayrak-Toydemir P. BMP9 mutations cause a vascular-anomaly syndrome with phenotypic overlap with hereditary hemorrhagic telangiectasia. *American journal of human genetics*. 2013;93:530-7.

5. Miller DT, Lee K, Chung WK, Gordon AS, Herman GE, Klein TE, Stewart DR, Amendola LM, Adelman K, Bale SJ, Gollob MH, Harrison SM, Hershberger RE, McKelvey K, Richards CS, Vlangos CN, Watson MS and Martin CL. ACMG SF v3.0 list for reporting of secondary findings in clinical exome and genome sequencing: a policy statement of the American College of Medical Genetics and Genomics (ACMG). *Genet Med*. 2021.

6. Barbara NP, Wrana JL and Letarte M. Endoglin is an accessory protein that interacts with the signaling receptor complex of multiple members of the transforming growth factor-beta superfamily. *J Biol Chem*. 1999;274:584-94.

7. Velasco S, Alvarez-Munoz P, Pericacho M, Dijke PT, Bernabeu C, Lopez-Novoa JM and Rodriguez-Barbero A. L- and S-endoglin differentially modulate TGFbeta1 signaling mediated by ALK1 and ALK5 in L6E9 myoblasts. *J Cell Sci*. 2008;121:913-9.

8. Calvo-Sánchez MI, Fernández-Martos S, Carrasco E, Moreno-Bueno G, Bernabéu C, Quintanilla M and Espada J. A role for the TGF-β/Bmp co-receptor Endoglin in the molecular oscillator that regulates the hair follicle cycle. *J Mol Cell Biol*. 2019;11:39-52.

9. Morikawa M, Koinuma D, Tsutsumi S, Vasilaki E, Kanki Y, Heldin CH, Aburatani H and Miyazono K. ChIP-seq reveals cell type-specific binding patterns of BMP-specific Smads and a novel binding motif. *Nucleic Acids Res*. 2011;39:8712-27.

10. Tual-Chalot S, Mahmoud M, Allinson KR, Redgrave RE, Zhai Z, Oh SP, Fruttiger M and Arthur HM. Endothelial depletion of Acvrl1 in mice leads to arteriovenous malformations associated with reduced endoglin expression. *PLoS One*. 2014;9:e98646.

11. Venkatesha S, Toporsian M, Lam C, Hanai J, Mammoto T, Kim YM, Bdolah Y, Lim KH, Yuan HT, Libermann TA, Stillman IE, Roberts D, D'Amore PA, Epstein FH, Sellke FW, Romero R, Sukhatme VP, Letarte M and Karumanchi SA. Soluble endoglin contributes to the pathogenesis of preeclampsia. *Nat Med*. 2006;12:642-9.

12. Hawinkels LJ, Kuiper P, Wiercinska E, Verspaget HW, Liu Z, Pardali E, Sier CF and ten Dijke P. Matrix metalloproteinase-14 (MT1-MMP)-mediated endoglin shedding inhibits tumor angiogenesis. *Cancer Res*. 2010;70:4141-50.

13. Jin Y, Muhl L, Burmakin M, Wang Y, Duchez AC, Betsholtz C, Arthur HM and Jakobsson L. Endoglin prevents vascular malformation by regulating flow-induced cell migration and specification through VEGFR2 signalling. *Nat Cell Biol*. 2017;19:639-652.

14. Sugden WW, Meissner R, Aegerter-Wilmsen T, Tsaryk R, Leonard EV, Bussmann J, Hamm MJ, Herzog W, Jin Y, Jakobsson L, Denz C and Siekmann AF. Endoglin controls blood vessel diameter through endothelial cell shape changes in response to haemodynamic cues. *Nat Cell Biol*. 2017;19:653-665.

15. David L, Mallet C, Mazerbourg S, Feige JJ and Bailly S. Identification of BMP9 and BMP10 as functional activators of the orphan activin receptor-like kinase 1 (ALK1) in endothelial cells. *Blood*. 2007;109:1953-61.

16. Derynck R and Budi EH. Specificity, versatility, and control of TGF-beta family signaling. *Sci Signal*. 2019;12.

17. Benzinou M, Clermont FF, Letteboer TG, Kim JH, Espejel S, Harradine KA, Arbelaez J, Luu MT, Roy R, Quigley D, Higgins MN, Zaid M, Aouizerat BE, van Amstel JK, Giraud S, Dupuis-Girod S, Lesca G, Plauchu H, Hughes CC, Westermann CJ and Akhurst RJ. Mouse and human strategies identify PTPN14 as a modifier of angiogenesis and hereditary haemorrhagic telangiectasia. *Nat Commun*. 2012;3:616.

18. Fu P, Ramchandran R, Shaaya M, Huang L, Ebenezer DL, Jiang Y, Komarova Y, Vogel SM, Malik AB, Minshall RD, Du G, Tonks NK and Natarajan V. Phospholipase D2 restores endothelial barrier function by promoting PTPN14-mediated VE-cadherin dephosphorylation. *J Biol Chem*. 2020;295:7669-7685.

19. Zhang P, Guo A, Possemato A, Wang C, Beard L, Carlin C, Markowitz SD, Polakiewicz RD and Wang Z. Identification and functional characterization of p130Cas as a substrate of protein tyrosine phosphatase nonreceptor 14. *Oncogene*. 2012.

20. Diaz-Valdivia NI, Diaz J, Contreras P, Campos A, Rojas-Celis V, Burgos-Ravanal RA, Lobos-Gonzalez L, Torres VA, Perez VI, Frei B, Leyton L and Quest AFG. The non-receptor tyrosine phosphatase type 14 blocks caveolin-1-enhanced cancer cell metastasis. *Oncogene*. 2020;39:3693-3709.

21. Wadham C, Gamble JR, Vadas MA and Khew-Goodall Y. The protein tyrosine phosphatase Pez is a major phosphatase of adherens junctions and dephosphorylates beta-catenin. *Mol Biol Cell*. 2003;14:2520-9.

22. Barr AJ, Debreczeni JE, Eswaran J and Knapp S. Crystal structure of human protein tyrosine phosphatase 14 (PTPN14) at 1.65-A resolution. *Proteins*. 2006;63:1132-6.

23. Barr AJ, Ugochukwu E, Lee WH, King ON, Filippakopoulos P, Alfano I, Savitsky P, Burgess-Brown NA, Muller S and Knapp S. Large-scale structural analysis of the classical human protein tyrosine phosphatome. *Cell*. 2009;136:352-63.

24. Wang W, Huang J, Wang X, Yuan J, Li X, Feng L, Park JI and Chen J. PTPN14 is required for the density-dependent control of YAP1. *Genes Dev*. 2012;26:1959-71.

25. Liu X, Yang N, Figel SA, Wilson KE, Morrison CD, Gelman IH and Zhang J. PTPN14 interacts with and negatively regulates the oncogenic function of YAP. *Oncogene*. 2012.

26. Huang JM, Nagatomo I, Suzuki E, Mizuno T, Kumagai T, Berezov A, Zhang H, Karlan B, Greene MI and Wang Q. YAP modifies cancer cell sensitivity to EGFR and survivin inhibitors and is negatively regulated by the non-receptor type protein tyrosine phosphatase 14. *Oncogene*. 2012.

27. Wilson KE, Li YW, Yang N, Shen H, Orillion AR and Zhang J. PTPN14 forms complex with Kibra and LATS1 proteins and negatively regulates the YAP oncogenic function. *The Journal of biological chemistry*. 2014.

28. Knight JF, Sung VYC, Kuzmin E, Couzens AL, de Verteuil DA, Ratcliffe CDH, Coelho PP, Johnson RM, Samavarchi-Tehrani P, Gruosso T, Smith HW, Lee W, Saleh

SM, Zuo D, Zhao H, Guiot MC, Davis RR, Gregg JP, Moraes C, Gingras AC and Park M. KIBRA (WWC1) Is a Metastasis Suppressor Gene Affected by Chromosome 5q Loss in Triple-Negative Breast Cancer. *Cell Rep*. 2018;22:3191-3205.

29. GTEx Consortium. Genetic effects on gene expression across human tissues. *Nature*. 2017;550:204-213.

30. Quigley DA, To MD, Perez-Losada J, Pelorosso FG, Mao JH, Nagase H, Ginzinger DG and Balmain A. Genetic architecture of mouse skin inflammation and tumour susceptibility. *Nature*. 2009;458:505-8.

31. Quigley DA, Kandyba E, Huang P, Halliwill KD, Sjolund J, Pelorosso F, Wong CE, Hirst GL, Wu D, Delrosario R, Kumar A and Balmain A. Gene Expression Architecture of Mouse Dorsal and Tail Skin Reveals Functional Differences in Inflammation and Cancer. *Cell Rep*. 2016;16:1153-1165.

32. Letteboer TG, Benzinou M, Merrick CB, Quigley DA, Zhau K, Kim IJ, To MD, Jablons DM, van Amstel JK, Westermann CJ, Giraud S, Dupuis-Girod S, Lesca G, Berg JH, Balmain A and Akhurst RJ. Genetic variation in the functional ENG allele inherited from the non-affected parent associates with presence of pulmonary arteriovenous malformation in hereditary hemorrhagic telangiectasia 1 (HHT1) and may influence expression of PTPN14. *Frontiers in Genetics*. 2015;6:67.

33. Kim IJ, Quigley D, To MD, Pham P, Lin K, Jo B, Jen KY, Raz D, Kim J, Mao JH, Jablons D and Balmain A. Rewiring of human lung cell lineage and mitotic networks in lung adenocarcinomas. *Nat Commun*. 2013;4:1701.

34. Jiang K, Liu P, Xu H, Liang D, Fang K, Du S, Cheng W, Ye L, Liu T, Zhang X, Gong P, Shao S, Wang Y and Meng S. SASH1 suppresses triple-negative breast

cancer cell invasion through YAP-ARHGAP42-actin axis. *Oncogene*. 2020;39:5015-5030.

35. Lu J, Hu Z, Deng Y, Wu Q, Wu M and Song H. MEKK2 and MEKK3 orchestrate multiple signals to regulate Hippo pathway. *J Biol Chem*. 2021;296:100400.

36. Durkin ME, Ullmannova V, Guan M and Popescu NC. Deleted in liver cancer 3 (DLC-3), a novel Rho GTPase-activating protein, is downregulated in cancer and inhibits tumor cell growth. *Oncogene*. 2007;26:4580-9.

37. Lin Y, Chen NT, Shih YP, Liao YC, Xue L and Lo SH. DLC2 modulates angiogenic responses in vascular endothelial cells by regulating cell attachment and migration. *Oncogene*. 2010;29:3010-6.

38. Cibi DM, Bi-Lin KW, Shekeran SG, Sandireddy R, Tee N, Singh A, Wu Y, Srinivasan DK, Kovalik JP, Ghosh S, Seale P and Singh MK. Prdm16 Deficiency Leads to Age-Dependent Cardiac Hypertrophy, Adverse Remodeling, Mitochondrial Dysfunction, and Heart Failure. *Cell Rep*. 2020;33:108288.

39. Mello SS, Valente LJ, Raj N, Seoane JA, Flowers BM, McClendon J, Bieging-Rolett KT, Lee J, Ivanochko D, Kozak MM, Chang DT, Longacre TA, Koong AC, Arrowsmith CH, Kim SK, Vogel H, Wood LD, Hruban RH, Curtis C and Attardi LD. A p53 Super-tumor Suppressor Reveals a Tumor Suppressive p53-Ptpn14-Yap Axis in Pancreatic Cancer. *Cancer Cell*. 2017;32:460-473.e6.

40. Wang Z, Shen D, Parsons DW, Bardelli A, Sager J, Szabo S, Ptak J, Silliman N, Peters BA, van der Heijden MS, Parmigiani G, Yan H, Wang TL, Riggins G, Powell SM, Willson JK, Markowitz S, Kinzler KW, Vogelstein B and Velculescu VE. Mutational analysis of the tyrosine phosphatome in colorectal cancers. *Science*. 2004;304:1164-6.

41. Travaglini KJ, Nabhan AN, Penland L, Sinha R, Gillich A, Sit RV, Chang S, Conley SD, Mori Y, Seita J, Berry GJ, Shrager JB, Metzger RJ, Kuo CS, Neff N, Weissman IL, Quake SR and Krasnow MA. A molecular cell atlas of the human lung from single-cell RNA sequencing. *Nature*. 2020;587:619-625.

42. Endale M, Ahlfeld S, Bao E, Chen X, Green J, Bess Z, Weirauch MT, Xu Y and Perl AK. Temporal, spatial, and phenotypical changes of PDGFRα expressing fibroblasts during late lung development. *Dev Biol*. 2017;425:161-175.

43. LungMap. The results are based upon data generated by the LungMAP Consortium [U01HL122642] and downloaded from (www.lungmap.net), on April 14th 2021. The LungMAP consortium and the LungMAP Data Coordinating Center (1U01HL122638) are funded by the National Heart, Lung, and Blood Institute (NHLBI).

. 2015.

44. Dickinson ME, Flenniken AM, Ji X, Teboul L, Wong MD, White JK, Meehan TF, Weninger WJ, Westerberg H, Adissu H, Baker CN, Bower L, Brown JM, Caddle LB, Chiani F, Clary D, Cleak J, Daly MJ, Denegre JM, Doe B, Dolan ME, Edie SM, Fuchs H, Gailus-Durner V, Galli A, Gambadoro A, Gallegos J, Guo S, Horner NR, Hsu CW, Johnson SJ, Kalaga S, Keith LC, Lanoue L, Lawson TN, Lek M, Mark M, Marschall S, Mason J, McElwee ML, Newbigging S, Nutter LM, Peterson KA, Ramirez-Solis R, Rowland DJ, Ryder E, Samocha KE, Seavitt JR, Selloum M, Szoke-Kovacs Z, Tamura M, Trainor AG, Tudose I, Wakana S, Warren J, Wendling O, West DB, Wong L, Yoshiki A, International Mouse Phenotyping C, Jackson L, Infrastructure Nationale Phenomin ICdlS, Charles River L, Harwell MRC, Toronto Centre for P, Wellcome Trust Sanger I, Center RB, MacArthur DG, Tocchini-Valentini GP, Gao X, Flicek P, Bradley A, Skarnes

WC, Justice MJ, Parkinson HE, Moore M, Wells S, Braun RE, Svenson KL, de Angelis MH, Herault Y, Mohun T, Mallon AM, Henkelman RM, Brown SD, Adams DJ, Lloyd KC, McKerlie C, Beaudet AL, Bucan M and Murray SA. High-throughput discovery of novel developmental phenotypes. *Nature*. 2016;537:508-514.

45. Baeyens N, Larrivee B, Ola R, Hayward-Piatkowskyi B, Dubrac A, Huang B, Ross TD, Coon BG, Min E, Tsarfati M, Tong H, Eichmann A and Schwartz MA. Defective fluid shear stress mechanotransduction mediates hereditary hemorrhagic telangiectasia. *J Cell Biol*. 2016;214:807-16.

46. Upton PD, Davies RJ, Trembath RC and Morrell NW. Bone morphogenetic protein (BMP) and activin type II receptors balance BMP9 signals mediated by activin receptor-like kinase-1 in human pulmonary artery endothelial cells. *J Biol Chem*. 2009;284:15794-804.

47. Goumans MJ, Valdimarsdottir G, Itoh S, Lebrin F, Larsson J, Mummery C, Karlsson S and ten Dijke P. Activin receptor-like kinase (ALK)1 is an antagonistic mediator of lateral TGFbeta/ALK5 signaling. *Mol Cell*. 2003;12:817-28.

48. Belle L, Ali N, Lonic A, Li X, Paltridge JL, Roslan S, Herrmann D, Conway JR, Gehling FK, Bert AG, Crocker LA, Tsykin A, Farshid G, Goodall GJ, Timpson P, Daly RJ and Khew-Goodall Y. The tyrosine phosphatase PTPN14 (Pez) inhibits metastasis by altering protein trafficking. *Science signaling*. 2015;8:ra18.

49. Park H, Furtado J, Poulet M, Chung M, Yun S, Lee S, Sessa WC, Franco CA, Schwartz MA and Eichmann A. Defective Flow-Migration Coupling Causes Arteriovenous Malformations in Hereditary Hemorrhagic Telangiectasia. *Circulation*. 2021.

50. Pawlikowska L, Nelson J, Guo DE, McCulloch CE, Lawton MT, Kim H and Faughnan ME. Association of common candidate variants with vascular malformations and intracranial hemorrhage in hereditary hemorrhagic telangiectasia. *Molecular genetics & genomic medicine*. 2018;6:350-356.

51. Sakabe M, Fan J, Odaka Y, Liu N, Hassan A, Duan X, Stump P, Byerly L, Donaldson M, Hao J, Fruttiger M, Lu QR, Zheng Y, Lang RA and Xin M. YAP/TAZ-CDC42 signaling regulates vascular tip cell migration. *Proc Natl Acad Sci U S A*. 2017;114:10918-10923.

52. Poduri A, Chang AH, Raftrey B, Rhee S, Van M and Red-Horse K. Endothelial cells respond to the direction of mechanical stimuli through SMAD signaling to regulate coronary artery size. *Development*. 2017;144:3241-3252.

53. Ola R, Kunzel SH, Zhang F, Genet G, Chakraborty R, Pibouin-Fragner L, Martin K, Sessa W, Dubrac A and Eichmann A. SMAD4 Prevents Flow Induced Arteriovenous Malformations by Inhibiting Casein Kinase 2. *Circulation*. 2018;138:2379-2394.

54. Crist AM, Lee AR, Patel NR, Westhoff DE and Meadows SM. Vascular deficiency of Smad4 causes arteriovenous malformations: a mouse model of Hereditary Hemorrhagic Telangiectasia. *Angiogenesis*. 2018;21:363-380.

55. Zhou Z, Tang AT, Wong WY, Bamezai S, Goddard LM, Shenkar R, Zhou S, Yang J, Wright AC, Foley M, Arthur JS, Whitehead KJ, Awad IA, Li DY, Zheng X and Kahn ML. Cerebral cavernous malformations arise from endothelial gain of MEKK3-KLF2/4 signalling. *Nature*. 2016;532:122-6.

56. Snodgrass RO, Chico TJA and Arthur HM. Hereditary Haemorrhagic Telangiectasia, an Inherited Vascular Disorder in Need of Improved Evidence-Based Pharmaceutical Interventions. *Genes (Basel)*. 2021;12.

57. Murphy NP, Mott HR and Owen D. Progress in the therapeutic inhibition of Cdc42 signalling. *Biochem Soc Trans*. 2021;49:1443-1456.

58. Team RC. R: A language and environment for statistical computing. . *R Foundation for Statistical Computing*. 2020.

59. topGO: Enrichment Analysis for Gene Ontology. [computer program]. 2021.

60. Genome wide annotation for Mouse [computer program]. Bioconductor.org; 2019.

61. gplots: Various R Programming Tools for Plotting Data [computer program]. 2020.

62. Burn SF. Detection of β-galactosidase activity: X-gal staining. *Methods Mol Biol*. 2012;886:241-50.

Methods:

Extraction of RNA From A *Mus Spretus* × *Mus Musculus* F1 backcross. All animal experiments were approved a priori by the UCSF IACUC. 69 F1.backcross mice were generated by crossing inbred male SPRET/Ei with inbred female FVB/N mice (Jackson Laboratory). Female F1 hybrids were then mated to male FVB/N mice. Lungs from eight-week-old mice were snap-frozen, and RNA was isolated usingTRIzol (Invitrogen) according to the manufacturer's instructions. Residual contaminating genomic DNA was removed by DNase treatment (Ambion). RNA was extracted with Trizol followed by DNAse I treatment and purification (RNeasy RNA purification kit,Qiagen).The purified RNA was quantified with Nanodrop and QC checked by Agilent Bioanalyzer.

Illumina Gene expression analysis

Gene expression was measured with the Illumina Mouse Whole Genome array (Illumina Inc.,San Diego,CA,USA). Sample preparations, hybridization and scanning were performed according to manufacturer's instructions. Briefly, 200ng of total RNA was prepared to make cRNA by using Illumina Total Prep RNA Amplification Kit (Ambion). First- strand complementary DNA was generated with T7 oligo(dT) primer and Array Script and then second cDNA was also made with DNA polymerase. Biotin-NTP with T7 enzyme mixes was used to make biotinylated cRNAs. The labeled cRNAs were purified, quantified and checked again using the Bioanalyzer. The labeled cRNA target was used for hybridization and scanning according to Illumina protocols. Probes with present/absent call ≥0.05 assessed by Illumina Bead studio software, were marked absent. Raw microarray data were quantile normalized and log2-transformed. Statistical analysis was performed with Rversion2.13[58].

Lung Gene Expression Correlation Analysis:

Lung gene expression correlation analysis was undertaken using the program Carmen[31].

GO Enrichment Analysis

In order to test for functional enrichment in gene clusters, we implemented R/topGO v2.44.0[59] on Biological Process using Fisher exact tests, correcting for multiple testing with the Benjamini-Hochberg procedure, using annotations provided by R/org.Mm.eg.db v3.8.2[60]. To capture an unbiased view of GO enrichment, in Figure 1D we display the top 10 most significantly enriched terms for each gene cluster according to FDR. We calculated enrichment scores as observed / expected within functional categories. We then centered and scaled across the matrix, generating a heatmap of the scaled scores using R/gplots/heatmap.2 v3.1.1[61].

Cell culture: Human Umbilical Arterial ECs (HUAEC) from LONZA® or PromoCell® were used between passage 1 to 3. They were cultured in EC specific medium with 2% FBS (EGMTM-2 EC Growth Medium-2 BulletKit™**,** LONZA® or EC Growth Medium 2, PromoCell®) at 10^5 cell/well in a 6 well plate. For over-expression studies, HEK293 cells (ATCC; CRL-1573™) were cultured in DMEM medium containing D-Glucose, L-Glutamine and Sodium pyruvate (GIBCO®), 10% FBS and 1% Penicillin/Streptavidin. For Proteasome inhibition using MG132 (M7449, SIGMA-Aldrich®) at 1µM in the culture media of HEK293 after cell transfection, cell were treated for 24 hours before the protein extraction.

Gene Expression Knock Down (KD): When the cells were 80% confluent, they were transfected with 0.006 pMol of siRNA (Dharmacon®) for each gene under study using

RNAi Max Lipofectamine (Invitrogen®) (**Supplementary Table S5**). 48h after transfection, cells were treated with 2 ng/ml BMP9 (R&D®) with no prior serum starvation since serum starvation reduced SMAD4 levels in HUAEC. At the stated end points post-treatment, cells were washed with PBS and lysed (200 µl) with M-PER Mammalian Protein (ThermoScientific®) plus 1x Protease inhibitor (cOmplete Mini EDTA, Roche®). Cells were detached using a scraper (on ice), sonicated to lyse for 3s (20 kHz, using the Q500 Sonicator). After centrifugation of 13, 000 rpm for 10 min at 4˚C, the supernatant was collected and stored at -20C for analysis.

Growth factor signaling: Confluent HUAEC cells in EC specific medium with 2% FBS were treated with 2 ng/ml BMP9 (Recombinant Human BMP-9 Protein, # 3209-BP, R&D®) and proteins extracted at specified time points after treatment. BMP9 signaling inhibition was performed using an ALK-1 kinase small molecule inhibitor K02288 5 µM (#S7359, Selleckchem®). TGFβ treatment was undertaken using 2ng/ml of Recombinant Human TGF-beta 1 Protein (#240-B, R&D®) and signaling specificity tested using the specific inhibitor for ALK5 kinase activity: SB431542 5 µM (#S1067, Selleckchem®).

Ectopic protein expression: HEK293 cells were cultured in DMEM (GIBCO®) with 10% FBS (VWR®) and 1% Penicillin/Streptavidin. The V5-tagged PTPN14 expression constructs described by Liu et al.[25] were used for PTPN14 over-expression studies. Flag-tagged SMAD4 (#80888, Addgene®), and HA tagged TAZ (#32839, Addgene®) cloned into pcDNA, were also used. Cells were transfected with 2.5 µg of plasmid per well of a 6-well plate using Lipofectamine 3000 (Invitrogen®) and protein expression levels analyzed 24h after transfection.

Western Blot: Western blot analysis was undertaken using 7.5% TGX gels (BioRad®) transferred onto 0.45 µm PVDF membranes (Amersham™ Hybond™, GE life science®). Transfer was undertaken using the BioRad® semi-dry system. After blocking the membrane for 1h at RT with AdvanBlock (Advansta®), and proteins were detected by incubation with relevant antibodies (**Supplementary Table S6**) diluted 1/500 in 2% BSA, followed by HRP-tagged secondary antibody (1/5000), in TBST 1x (CellSignaling®). Signal was detected using SuperSignal™ West Femto Maximum Sensitivity Substrate (Thermo Scientific™), and images captured using a ChemiDoc Imaging System (BioRad®).

Co-immuno-precipitation: Protein (10 µg) was immuno-precipitated using a target antibody (1 µg) with Pierce™ Protein A/G Magnetic Beads. Protein elution was undertaken using 1x LD Laemmli Sample Buffer (BioRad®) and denaturized at 95˚C for 5 minutes before transferring to ice before gel loading.

Nuclear cytoplasmic fraction: Cell fractionation was performed using NE-PER™ Nuclear and Cytoplasmic Extraction Reagents (Thermo Fisher™) and lysates were analyzed by Western-blot and/or used for Co-IP.

Dual Luciferase activity test:

HEK293 cell were transfected with pGL3BRE Luciferase (#45126, Addgene®) and pCMV-Renilla luciferase plasmid (Thermofisher #16153). Cells were transiently transfected with PTPN14 V5 tagged expression constructs[25] , after 24 hours cell are treated with BMP9 (2ng/ml) or combined to K02288 at 1µM (ALK-1 kinase inhibitor) and relative luciferase activities quantified after 16 hours using the Dual-Glo® Luciferase Assay System (Promega®). TGFβ Reporter Assay performed in TMLC stably

expressing the responding elements, after 16h treatment with TGFβ (2ng/ml) or combined to SB431542 (1μM) (ALK5 kinase inhibitor) and relative luciferase activities quantified after 16 hours using the Dual-Glo® Luciferase Assay System (Promega®) Histogram were generated and data analyzed by multiple paired t-test and 2-way ANOVA test using GraphPad (PRISM® 9.0.0).

Proximity Ligation Assay (PLA): PLA was undertaken on confluent primary HUAEC monolayers using the Duolink Proximity Ligation Assay (PLA) from Sigma. Anti-PTPN14 (Sigma Prestige) and anti-SMAD4 (Invitrogen) antibodies were used as primaries, and secondary anti-antibodies against the primaries were tagged with PLA probes. DNA ligation was carried out for 30 minutes at 37ºC with two circle-forming fluorescently-labelled DNA oligonucleotides and DNA ligase. PCR amplification of the PLA probes was enabled by incubation for 100 minutes at 37ºC. Cells were counterstained with DAPI for nuclear stain. Imaging at 40X was undertaken using a Keyence microscope.

RNAScope *in situ* hybridization: *In situ* hybridization was undertaking using standard protocols and reagents from the RNAScope 2.5 HD Duplex Detection Kit (Advanced Cell Diagnostics). Wild type C57BL/6J 8.5 dpc embryos, and adult lung and heart were fixed in 4% paraformaldehyde and embedded in paraffin. 5uM sections were used. Differentially-labelled RNA-specific oligonucleotide probes for *Eng* and *Ptpn14* were hybridized simultaneously, and chromogenic signals were detected at 10X and 40X by standard bright-field microscopy using a Keyence microscope.

Tissue β-galactosidase staining: X-Gal staining was carried out as described by Burn 2012[62]. We utilized *Ptpn14.tm1(KOMP)Vlcg* mice (MGI:5051040), henceforth termed *Ptpn14-LacZ*, a transgenic line harboring a *Ptpn14* gene reporter encoding β-

galactosidase expression from the endogenous *Ptpn14* gene promoter, that is essentially a *Ptpn14-null* allele. Harvested tissues were fixed with 0.2% glutaraldehyde in PBS for two hours at room temperature before being washed with PBS and treated with the X-Gal reagent, $K_4[Fe(CN)_6]$, and $K_3[Fe(CN)_6]$ at room temperature overnight. Tissues were washed with PBS the following day, fixed with 4% paraformaldehyde at room temperature for two hours and then embedded in Tissue Tek™ OCT compound and frozen on dry ice. Cryomolds were stored at -80ºC before cutting 10µM cryosections. Hematoxylin and eosin staining was performed per standard protocol. Imaging at 20X and 100X was by standard bright-field microscopy using a 6D/high throughput Nikon Ti inverted microscope.

Figure Legends

Figure 1: *Ptpn14* expression in lung correlates with markers of angiogenesis and vascular remodeling. A: Cartoon depicting the inter-specific backcross (*Mus spretus* x *Mus musculus*) F2 mice were generated from backcrossing male F1 hybrid mice to female *Mus musculus* FVB mice, and bulk RNAs harvested from individual lungs of 69 wildtype, genetically-distinct, mice. **B:** Venn diagram shows overlap of *Ptpn14*-correlated genes with those correlated with *Acvrl1* and with *Eng* in the 69-lung panel at *rho* ≥ 0.54. **C:** The 47 genes co-correlated with *Ptpn14, Eng,* and *Acvrl1* (Figure 1B) is presented as an Ingenuity Pathways Network generated based on preexisting knowledge of connectivity between genes. 13 of the 47 genes that correlated with *Smad4* (*rho ≥ 0.54*) are circled in red, and the four seed genes, *Ptpn14, Acvrl1, Eng, and Smad4,* are circled in black. **D.** Heat map indicating the magnitude of each pair-wise correlation coefficient between each of the 150 *Ptpn14*-associated genes compared with each other. Data underwent unsupervised hierarchical cluster analysis based on *rho* value for each pair-wise gene comparison. This reveals four gene clusters labelled A to D. **C:** Gene Ontology analysis for each of the four clusters found in **D.**

Figure 2: *Ptpn14* expression in ECs of multiple tissues. *Ptpn14* (cyan) and *Eng* (pink) RNA localization by RNAScope® in tissues harvested from C57BL/6J mice. (**A,B**) 8.5 dpc embryo; *Ptpn14* RNA localizes to embryonic neuroepithelium (NE) and extraembryonic yolk sac vessels and blood islands (YSV). (**C,D**) In lung, *Ptpn14* and *Eng* co-localize to the pulmonary blood vessels (BV), and *Ptpn14* but not *Eng* is expressed in bronchiolar epithelium (BE). A, alveoli. Br, bronchiole. (**E,F**) In heart,

Ptpn14 and *Eng* co-localize to endocardial cells (ECs) lining the left atrium (LA) and capillary ECs of the myocardium, such as within the interventricular septum (IVS) and left ventricle (LV). All tissues were counterstained with hematoxylin (RNAScope). Asterisks denote cells labeled with both *Eng* and *Ptpn14* probes.

Figure 3. Detection of endogenous *PTPN14* gene promoter activity *in vivo.*

(**A**) Section of lung, showing *Ptpn14-LacZ* expression in lymphatic endothelium (LE; black arrows). (**B**) High power image of area marked in (**A**). (**C**) Lung, showing *Ptpn14-LacZ* expression in a blood vessel (black arrow) and monocyte (grey arrow). (**D,E**) *Ptpn14-LacZ* in artery, veins, and capillaries of subcutaneous muscle. (**F**) *Ptpn14-LacZ* expression localized to subcutaneous blood vessel in adipose tissue (Ad). Red blood cells appear within vessel lumen. (**G**) Semilunar heart valve, showing *Ptpn14-LacZ* expression on the aortic side of the valve leaflet (black arrow), and within a vessel within the myocardium. (**H**) Heart, showing *Ptpn14-LacZ* localized to a coronary vessel, with red blood cells visible in the lumen. Ao, aorta; Ar, artery; AV, aortic valve leaflet; Br, bronchiole; C capillary; LE, lymphatic endothelium; LV, left ventricle; M, myocardium; PV, pulmonary vein; V, vein. All tissues were counterstained H&E.

Figure 4: Effects of *siPTPN14* on primary human EC protein expression. **A:** Sub-confluent HUAECs were transfected with specified *siRNAs,* protein lysates were harvested 48 hours later, following the indicated treatments for 0, 1 or 24 hours with BMP9 (2ng/ml), and assayed by Western blot (left) with **B:** Histograms (right) showing quantification of proteins relative to *siNT*-transfected HUAECs. **C:** Schematic of BMP9-

ALK-1-SMAD4 signaling. **D&E**: Western blot from HUAEC treated with 2ng/ml of BMP9 for 24h using siNT compared to siPTPN14 showing the effect of PTPN14 on Endoglin and SMAD4 level with the quantification graph (**E**). **F**: siRNA-treated cells Western blot of HUAECs cell lysates after 1h treatment with TGFβ (2ng/ml) or BMP9 (2ng/ml), with or without 5uM K02288 (an ALK-1 inhibitor) or 5uM SB431542 (a TGFβR1 inhibitor) with the observation of SMAD4, pSMAD1 and total Smad1 level trough the different conditions. **G:** Co-immunoprecipitation of endogenous PTPN14, SMAD4, Endoglin, ALK-1 SMAD7, or IgG control, shows interaction between endogenous PTPN14 and SMAD4,but not with Endoglin, ALK-1 and, SMAD7. **H:** SMAD4 pulldown with SMAD4, TAZ, pTAZ, pSAMD1/5, and SMAD7 is showing the interaction of SMAD4 with the different proteins.

Figure 5: PTPN14 binds and regulates SMAD4 levels. **A:** Western blot analyses showing *siPTPN14* effects on endoglin, SMAD4 and TAZ levels in nuclear and cytoplasmic HUAEC fractions, without BMP9 treatment. Calnexin and LaminB1 are cytoplasmic and nuclear markers, respectively. **B**: Western blot from HUAEC cell treated with BMP9 for 1h shoes the absence of PTPN14 protein reduces the level of SMAD4 but without blocking the translocation from the cytoplasm to the nucleus Calnexin and LaminB1 are cytoplasmic and nuclear markers, respectively.
C: Western blot analysis and reciprocal co-immunoprecipitation of transiently transfected HEK293 cells with SMAD4-FLAG compared to a combination increasing quantities of V5-PTPN14, visualized using anti-V5 and anti-Flag antibodies. Note, stabilization of SMAD4-FLAG protein by PTPN14 (left) and physical association

between the two proteins (right). **D:** Western blot analysis of cytoplasmic, and nuclear fractions (left to right) of HEK293 cell lysates after co-transfection of V5-PTPN14 and SMAD4-FLAG, showing stabilization of SMAD4 predominantly in the nuclear fraction. **E:** Co-immuno-precipitation of HEK293 cytoplasmic, and nuclear lysates (left to right) with an anti-FLAG antibody after co-transfection of V5-PTPN14 and SMAD4-FLAG, showing their physical interaction predominantly within the nucleus.

Figure 6: Physical association between PTPN14 and SMAD4 revealed by PLA. PLA was undertaken to investigate interactions between endogenous proteins in low passage HUAECs, as described in methods. PLA using anti-pSMAD1/5 with SMAD4 antibodies (**A,B**), or anti-PTPN14 with anti-SMAD4 antibodies (**C,D**), without (**A,C**) or after (**B,D**) 60 minutes exposure to 2ng/ml BMP9. Negative controls show PLA undertaken with one antibody only (**E-G**) or with secondary antibodies only (**H**).

Figure 7: Mutational analysis of PTPN14 indicates competition between SMAD4 and TAZ for binding. A: Schematic representation PTPN14 primary structure and different mutant constructs used. **B-C**: Western Blot analysis of HEK293 cell lysates co-transfected with SMAD4-FLAG and increasing levels of the different PTPN14 constructs as indicated ($PTPN14^{WT}$, ΔFERM, mPPxY, and ΔPTP). **D:** Quantification of differing SMAD4-FLAG levels according to co-transfection with different PTPN14 mutants (Data averaged from 3 different experiments). **E:**Representatife graph of BRE-Luciferase reporter assay in HEK293 to show the effects of different PTPN14 constructs on basal and BMP9-induced Luciferase-expression. H: PAI-1 -Luciferase reporter assay in

TMLC to show the effects of different PTPN14 expression on basal and TGFβ-induced Luciferase-expression. **G**: Western blot analysis to show the effects of V5-PTPN14 wild type and mPPxY.PTPN14 on co-transfected TAZ-HA levels. **H**: Western blot analysis of HEK293 cells co-transfected with V5-PTPN14 wild type or m PPxY.PTPN14, with and without SMAD4-FLAG and TAZ-HA to demonstrate the effect of TAZ on SMAD4 stability when co-transfected with PTPN14 that can (Wildtype) or cannot (mPPXY) bind to TAZ.

A

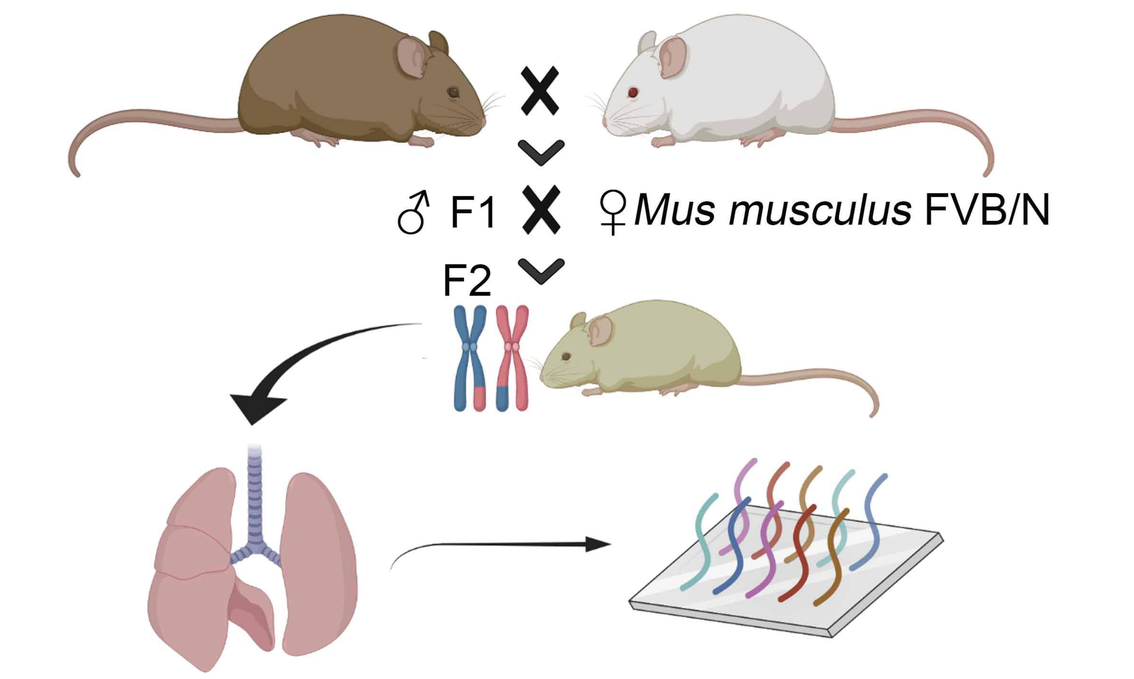
Mus spretus x Mus musculus FVB/N
♂ F1
♀Mus musculus FVB/N
F2
RNA from 69 genetically diverse mouse lungs
Micro-Array & gene expression correlation analysis

B

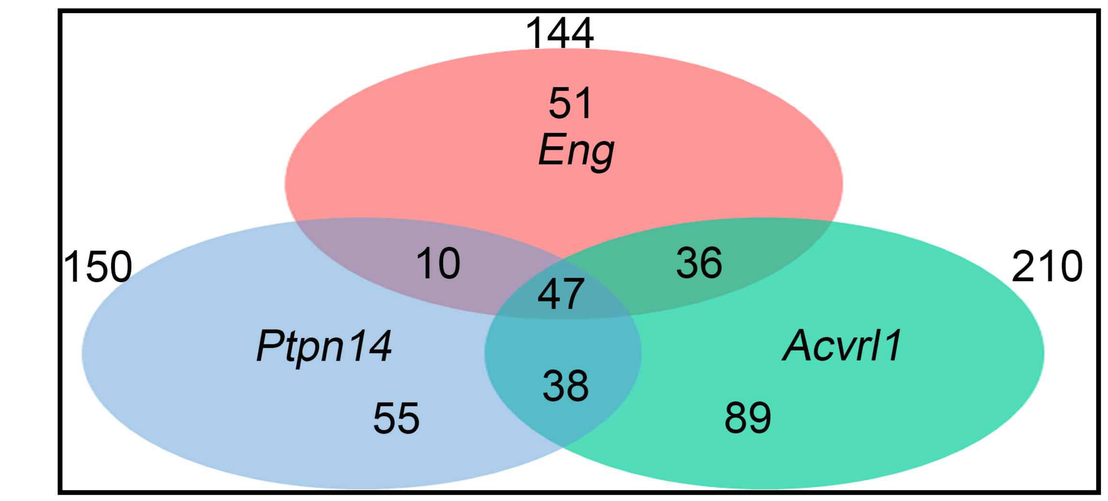
144
51
Eng
150
10
36
210
47
Ptpn14
Acvrl1
38
55
89

C

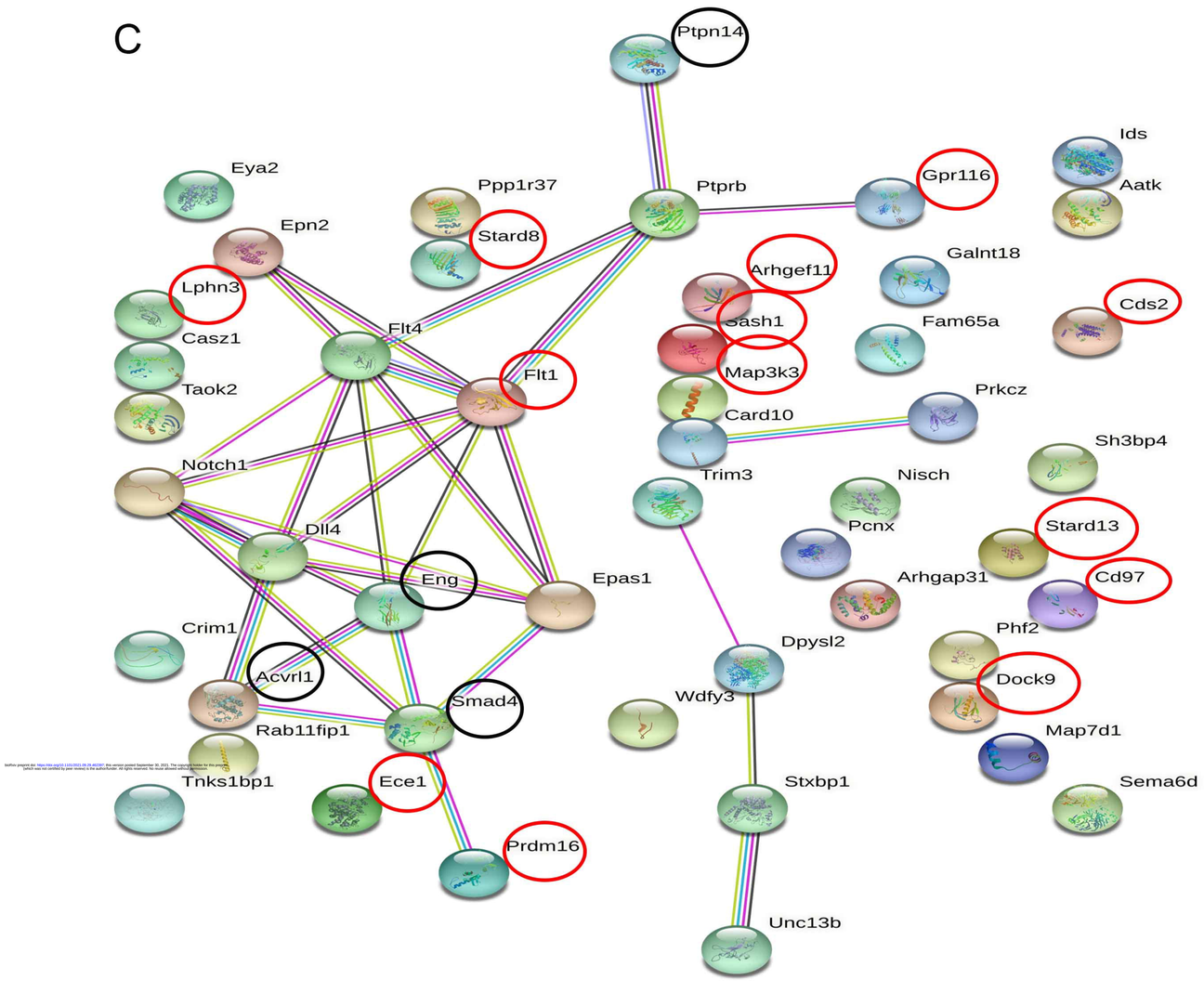
Ptpn14
Ptprb
Eya2
Epn2
Ppp1r37
Stard8
Lphn3
Casz1
Taok2
Flt4
Flt1
Notch1
Dll4
Eng
Epas1
Crim1
Acvrl1
Smad4
Rab11fip1
Tnks1bp1
Ece1
Prdm16
Gpr116
Ids
Aatk
Galnt18
Arhgef11
Sash1
Map3k3
Fam65a
Cds2
Card10
Prkcz
Trim3
Sh3bp4
Nisch
Pcnx
Stard13
Arhgap31
Cd97
Phf2
Dpysl2
Dock9
Wdfy3
Map7d1
Stxbp1
Sema6d
Unc13b

D

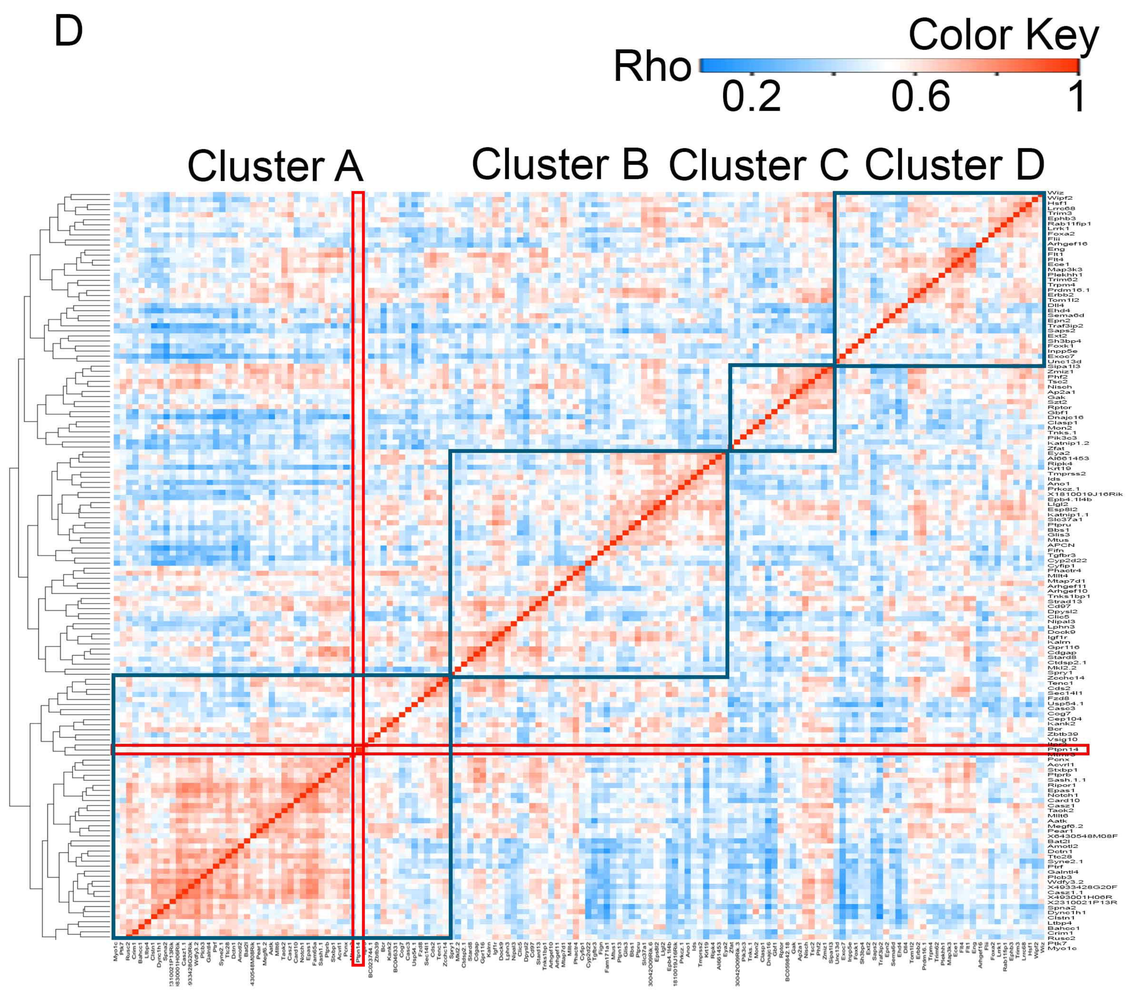
Color Key
Rho
0.2
0.6
1
Cluster A
Cluster B
Cluster C
Cluster D

E

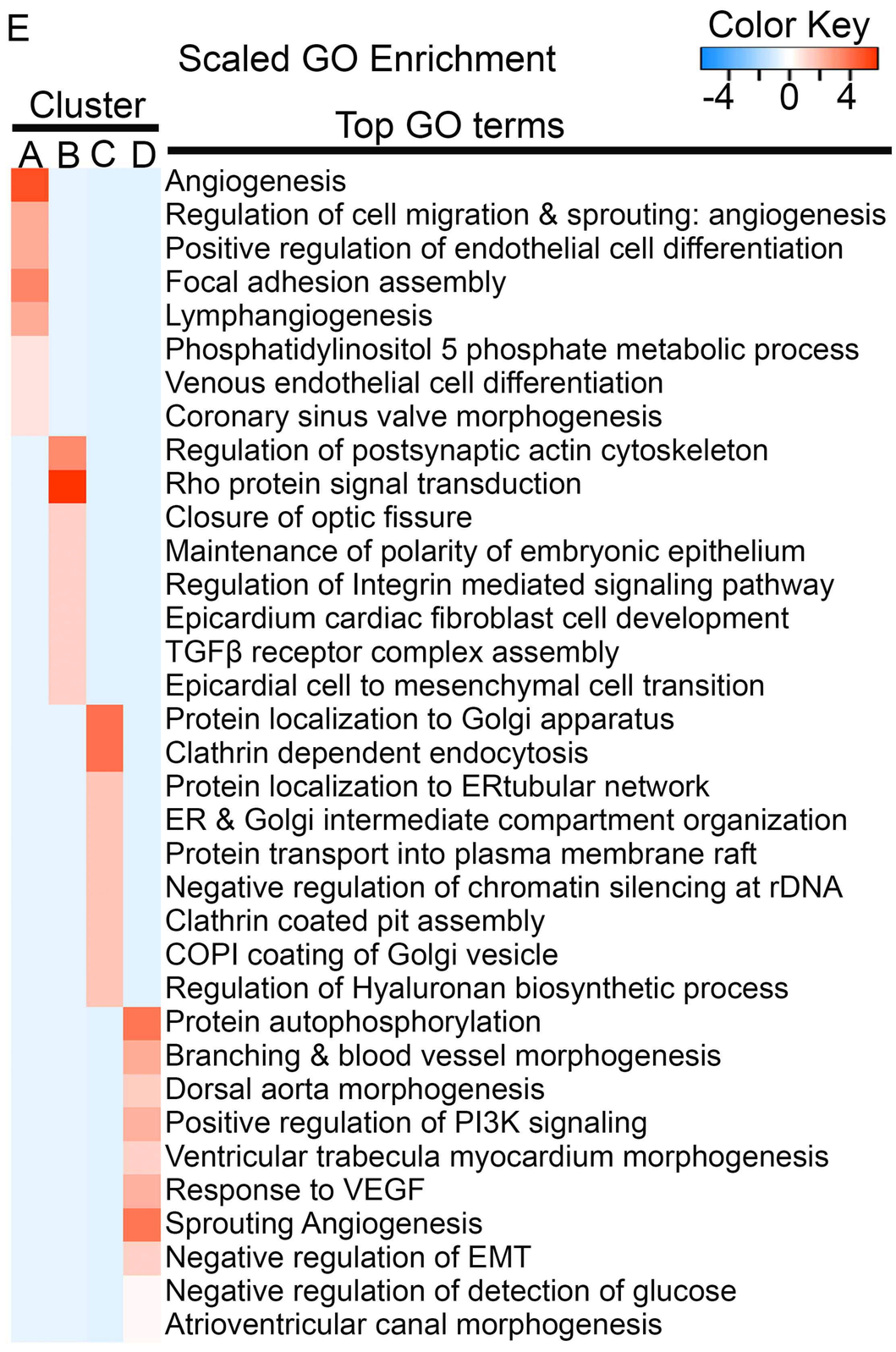
Scaled GO Enrichment
Color Key
-4
0
4
Cluster
A B C D
Top GO terms
Angiogenesis
Regulation of cell migration & sprouting: angiogenesis
Positive regulation of endothelial cell differentiation
Focal adhesion assembly
Lymphangiogenesis
Phosphatidylinositol 5 phosphate metabolic process
Venous endothelial cell differentiation
Coronary sinus valve morphogenesis
Regulation of postsynaptic actin cytoskeleton
Rho protein signal transduction
Closure of optic fissure
Maintenance of polarity of embryonic epithelium
Regulation of Integrin mediated signaling pathway
Epicardium cardiac fibroblast cell development
TGFβ receptor complex assembly
Epicardial cell to mesenchymal cell transition
Protein localization to Golgi apparatus
Clathrin dependent endocytosis
Protein localization to ERtubular network
ER & Golgi intermediate compartment organization
Protein transport into plasma membrane raft
Negative regulation of chromatin silencing at rDNA
Clathrin coated pit assembly
COPI coating of Golgi vesicle
Regulation of Hyaluronan biosynthetic process
Protein autophosphorylation
Branching & blood vessel morphogenesis
Dorsal aorta morphogenesis
Positive regulation of PI3K signaling
Ventricular trabecula myocardium morphogenesis
Response to VEGF
Sprouting Angiogenesis
Negative regulation of EMT
Negative regulation of detection of glucose
Atrioventricular canal morphogenesis

A *WT* embryo 8.5 dpc

NE

YSV

500 µM

B Yolk sac vessel

100 µM

C Lung

A

Br

Br

500 µM

D Lung

A

BE

Br

Br

100 µM

E Heart

LA

IVS

LV

500 µM

F Left atrium

50 µM

A Lung

PV

LE

LE

LE

LE

LE

Br

100 µM

B Lung

LE

25 µM

C Lung

50 µM

D Subcutaneous muscle

M

V

Ar

LE

M

V

M

100 µM

E Subcutaneous muscle

V

LE

Ar

50 µM

F Subcutaneous fat

Ad

100 µM

G Heart

Ao

Ar

M

AV

LV

100 µM

H Heart

CV

M

100 µM

Expression of endogenous proteins in HUAECs

A

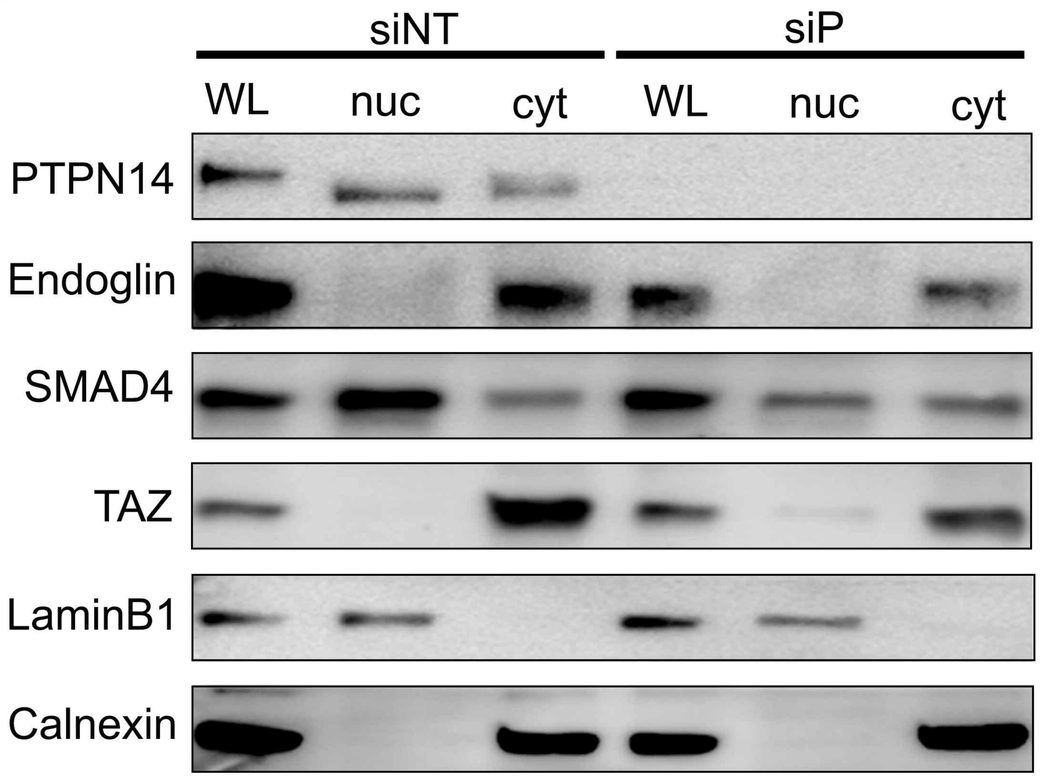

B

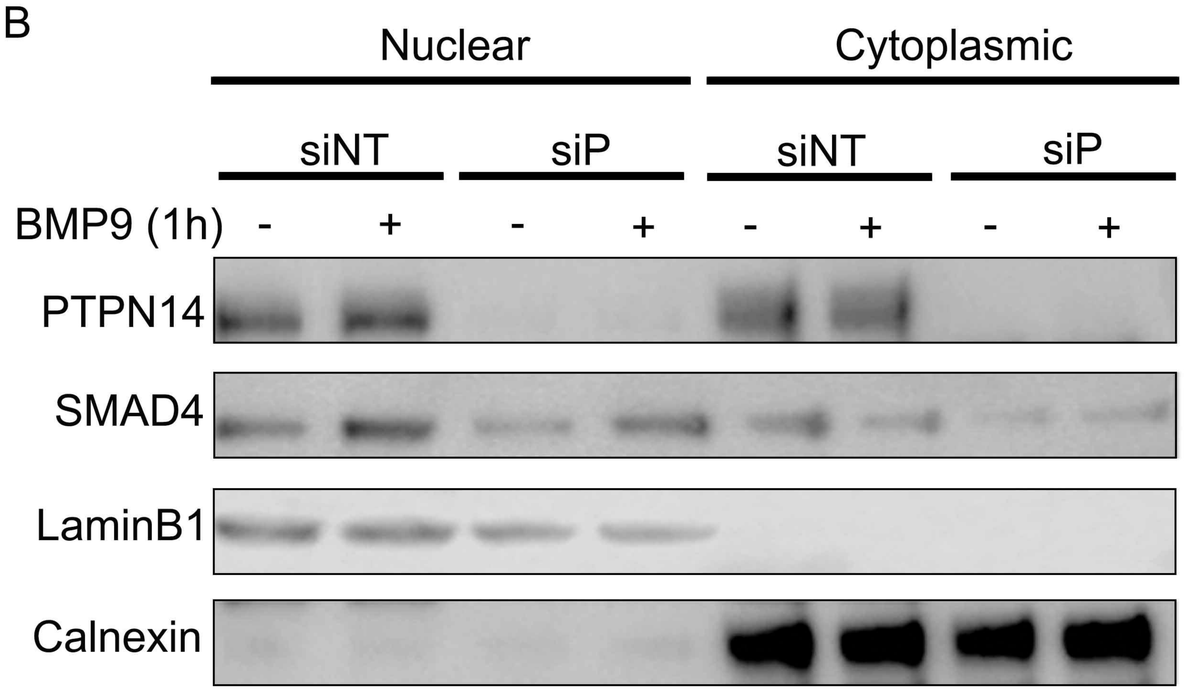

C

Expression of ectopic proteins in HEK293 cells

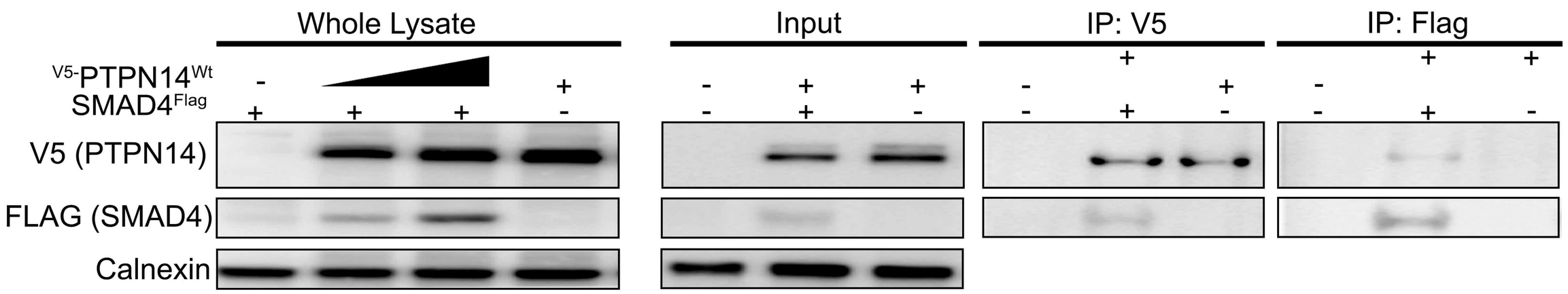

D

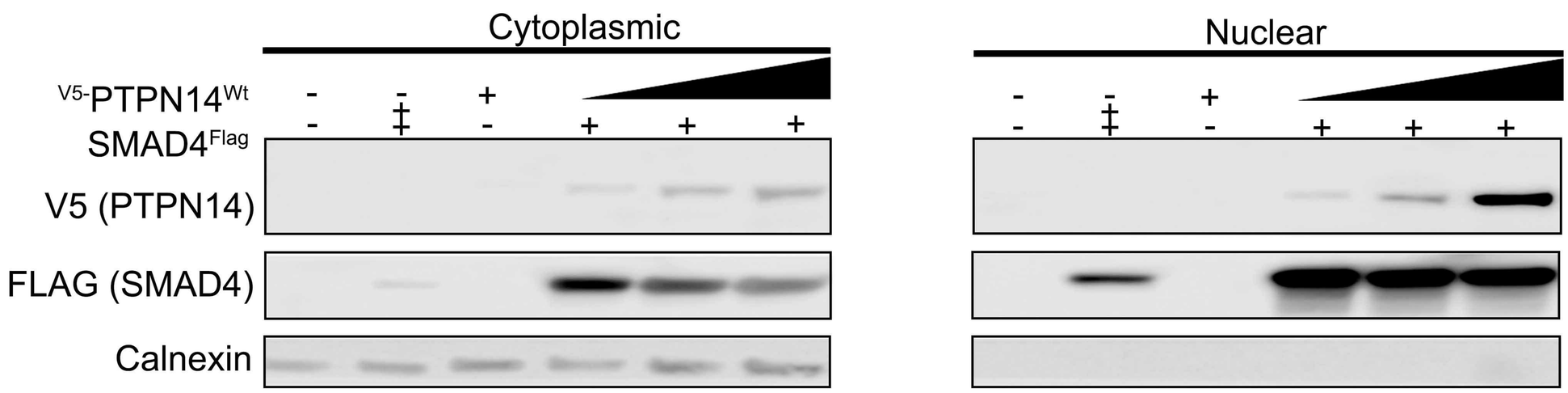

E

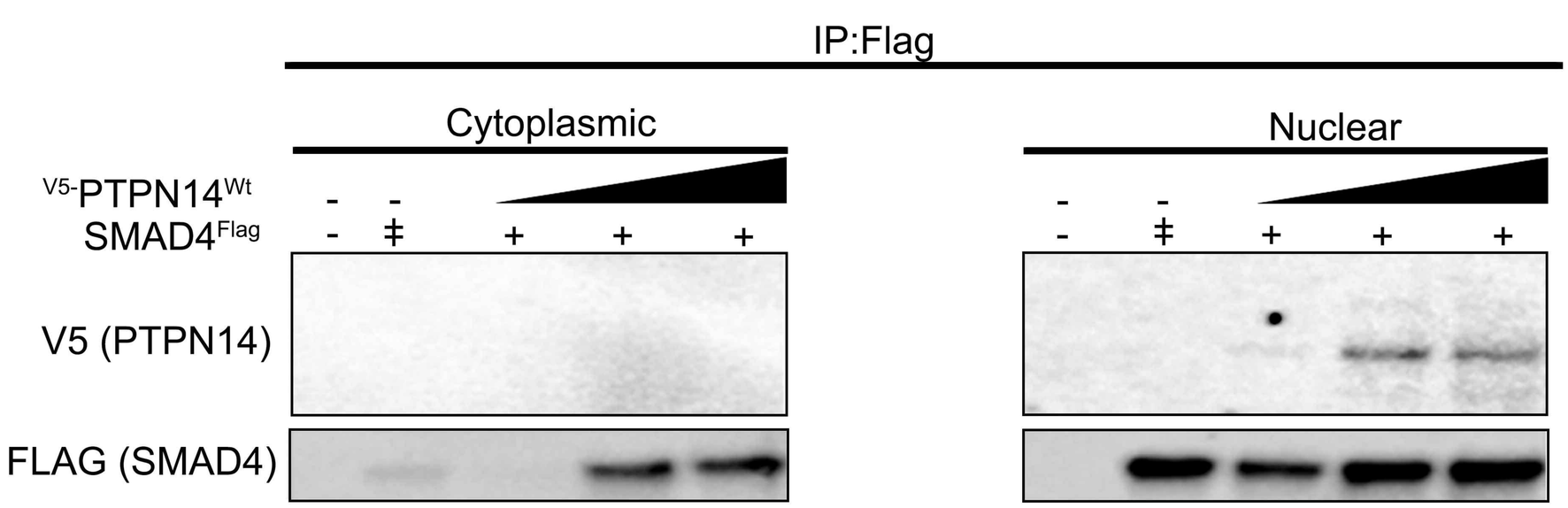

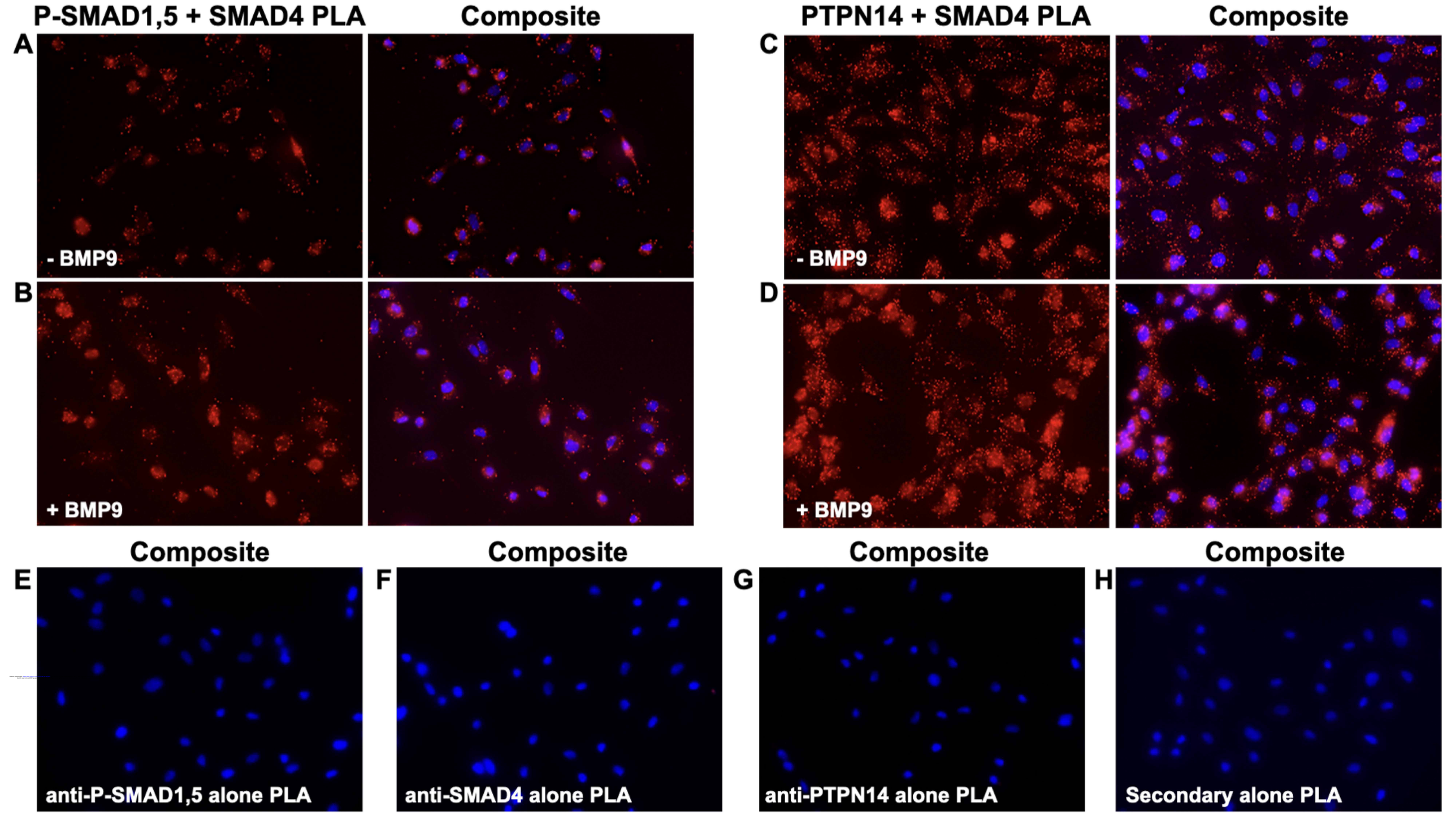
P-SMAD1,5 + SMAD4 PLA
Composite
PTPN14 + SMAD4 PLA
Composite
A
- BMP9
B
+ BMP9
C
- BMP9
D
+ BMP9
Composite
Composite
Composite
Composite
E
anti-P-SMAD1,5 alone PLA
F
anti-SMAD4 alone PLA
G
anti-PTPN14 alone PLA
H
Secondary alone PLA

A

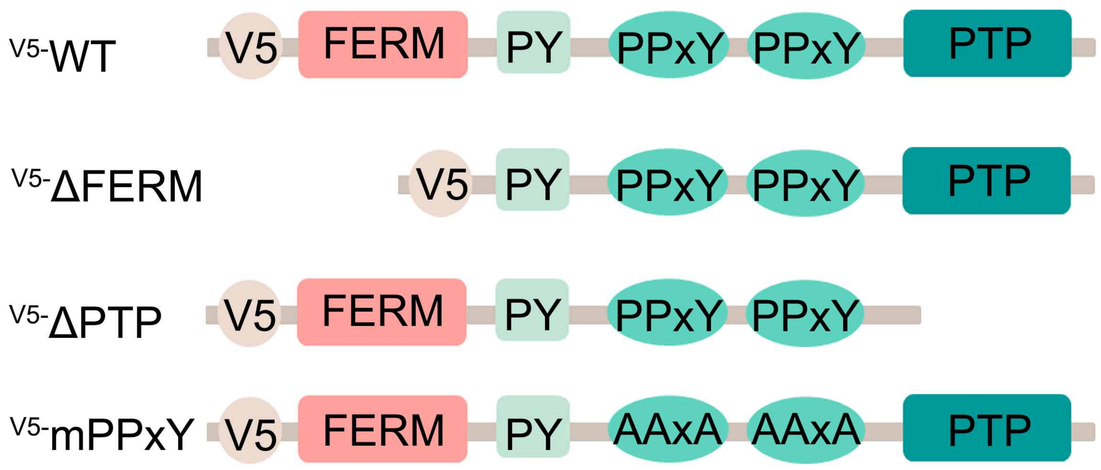

B

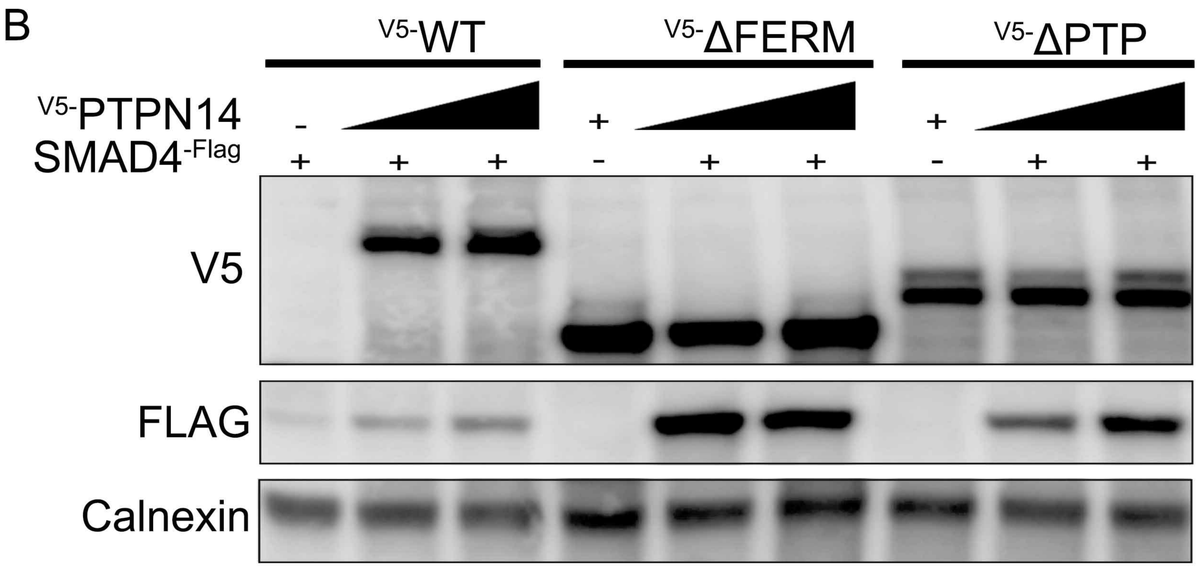

C

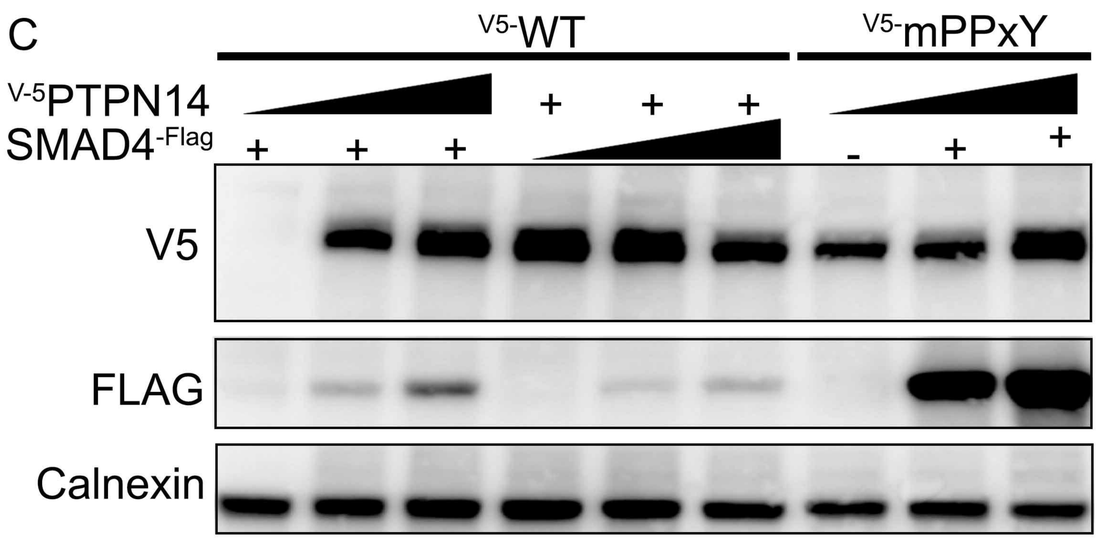

D

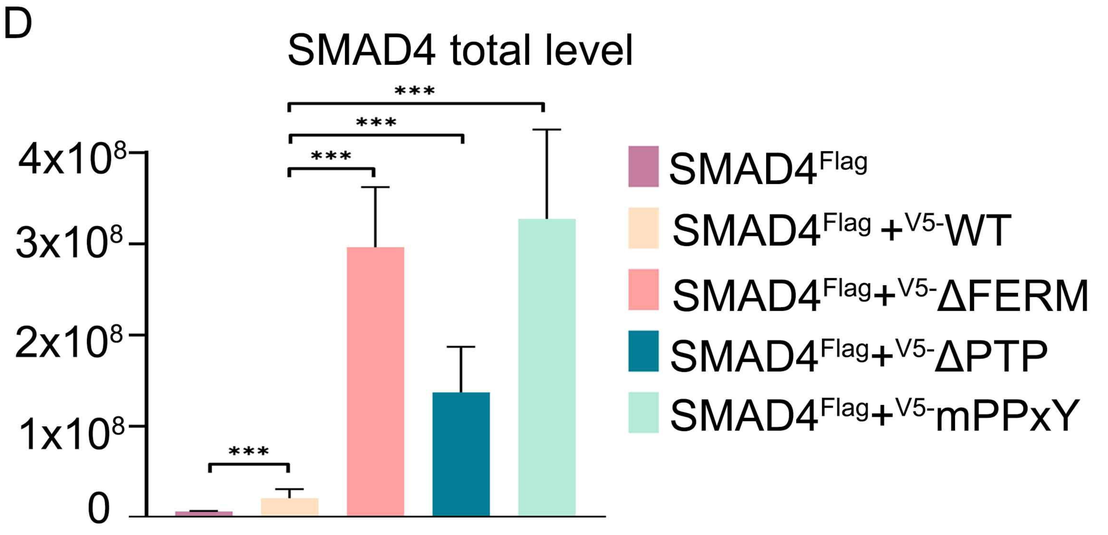

E

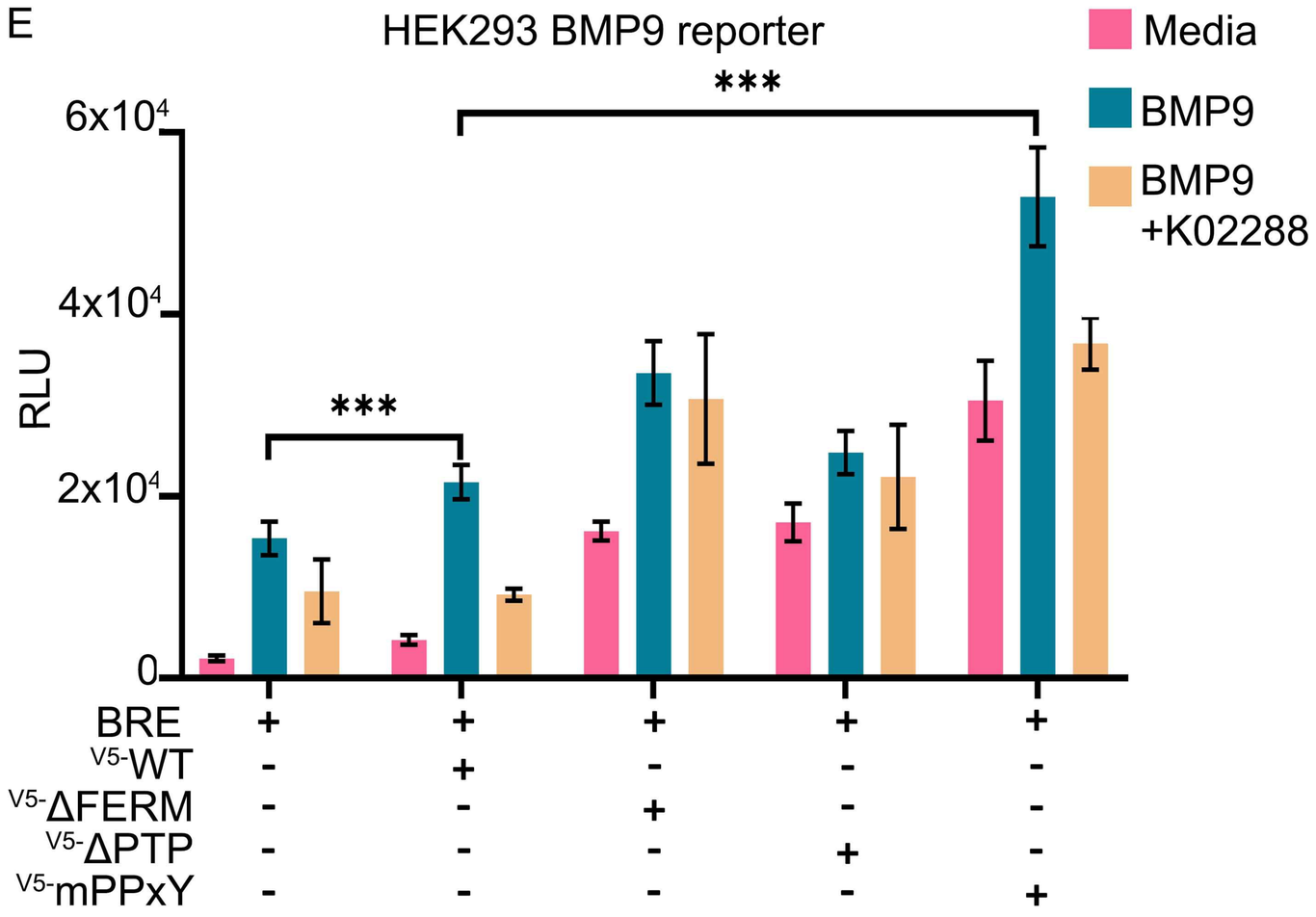

F

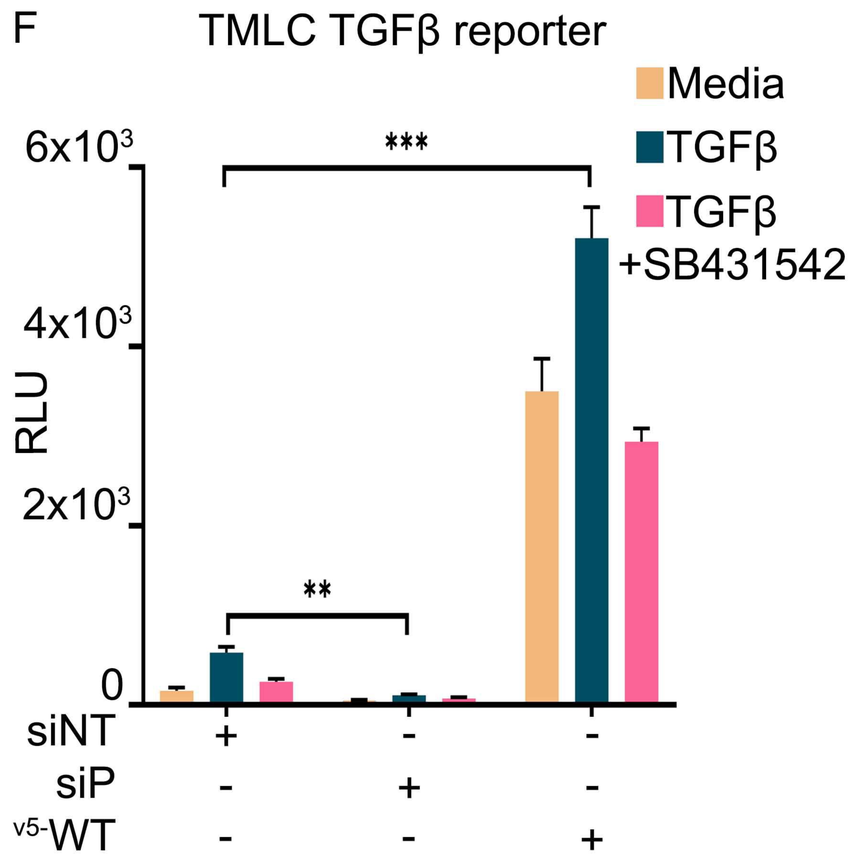

G

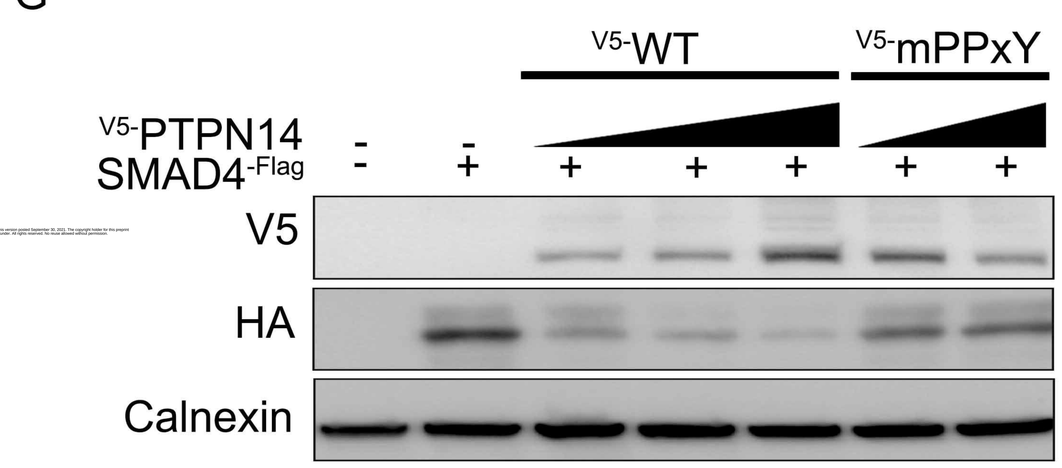

H